# Radar Altimeter Absolute Calibration Using GPS Water Level Measurements

by

Kai-chien Cheng

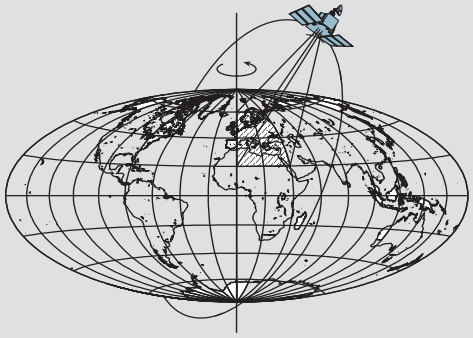

Report No. 469

Geodetic and GeoInformation Science
Department of Civil and Environmental Engineering and Geodetic Science
The Ohio State University
Columbus, Ohio  43210-1275

January 2004

# Radar Altimeter Absolute Calibration Using GPS Water Level Measurements

Kai-chien Cheng

Report No. 469

Geodetic and GeoInformation Science
Department of Civil and Environmental Engineering and Geodetic Science
The Ohio State University
Columbus, Ohio 43210-1275, USA

January 2004

ABSTRACT

Recent studies of using long-term island and coastal tide gauges (over 60 years) indicate that the global sea level rise is at a rate of 1.8 to 1.9 ± 0.1 mm/year (e.g., Douglas 1997, 1991; Trupin and Wahr, 1990; Warrick and Oerlemans, 1990). Satellite radar altimetry has evolved into a tool for synoptic observation of the global (±81.5° latitude) oceanic phenomena with unprecedented accuracy (several cm in sea surface height) and with a temporal resolution of 1-2 weeks and a spatial resolution of 50 km. Its accuracy, global coverage, and temporal resolution enable its use in studies of global sea level changes. With accurate links among different satellite radar altimeters, a decadal (~ 15 years) altimeter sea surface height (ssh) measurements can be obtained. However, the limitations of using altimeters to measure sea level include inadequate knowledge of the instrumental biases and their potential drifts of each individual radar altimeter.

The inherent requirements to enable the use of radar altimeters to measure global ssh include knowledge of the altimeter biases to within 1-cm accuracy and their drifts to less than 1 mm per year. The mechanism is to conduct the absolute radar altimeter calibration with the eventual goal to obtain the knowledge of its bias and drift with sufficient accuracy for sea level studies. The goal of the radar altimeter absolute calibration is to determine the altimeter bias and drift by comparing the altimeter-measured ssh with the accurate ground truth, often referred to as in situ data sets. However, both systems contain different error sources and it is necessary to formulate a closure equation and solved for the altimeter bias and drift with least squares.

In this paper, a GPS buoy campaign in Lake Michigan was conducted by the Laboratory for Space Geodesy and Remote Sensing Research of the Department of Civil and Environmental Engineering and Geodetic Science, at the Ohio State University (CEEGS/OSU) in cooperation with the National Geodetic Survey, National Oceanic and Atmospheric Administration (NGS/NOAA) from March 20 to 24, 1999. The lake was chosen because of the relatively calm water conditions such as waves and wind compared with oceans. 1-Hz kinematic data obtained from a GPS buoy and the lake level record from 1993 to 1999 collected by the Holland West tide gauge were used in this study as the in situ data sets for the absolute calibration of TOPEX/POSEIDON Side A (TSA) and Side B (TSB).

The GPS buoy and the Holland West tide gauge have not yet met the required accuracy of absolute radar altimeter calibration. The geoid gradient is the most dominant error source

among others and it should be carefully avoided. The T/P bias and drift estimations in this study are inaccurate because of the large geoid gradient in using GPS buoy data and the 10-cm discrepancy in using the Holland West tide gauge data. However, it can be anticipated that the accuracy will be improved with more data in the future and also with more data collected by other calibration sites worldwide.

# PREFACE

The report was prepared by Kai-chien Cheng, a graduate research associate in the Department of Civil and Environmental Engineering and Geodetic Science, at the Ohio State University, under the supervision of Professor C. K. Shum. This report was supported in part by the National Oceanographic Partnership Program Grant (Dynalysis of Princeton #865618) and National Aeronautics and Space Administration TOPEX/POSEIDON Extended Mission Grant (NAG5-6910/JPL961462), National Aeronautics and Space Administration Earth Science Information Partnership CAN Grant (CIT #12024478), National Aeronautics and Space Administration Interdisplanary Science Project (NAG5-9335), National Science Foundation Digital Government Grant (EIA-0091494, and the Ohio Sea Grant Program (R/CE-5).

This report was also submitted to the Graduate School of the Ohio State University as a thesis in partial fulfillment of the requirements for the Master of Science degree

ACKNOWLEDGMENT

I would like to express my gratitude and appreciation to Dr. C. K. Shum, my adviser, for his encouragement and inspiring consultation. This report would have not been possible without his help. I would also like to thank Dr. Christopher Jekeli and Dr. Yuchan Yi, who are in my Master Thesis Committee, for their valuable comments and suggestions. I acknowledge the help from Dr. Gerald Mader and Mr. Doug Martin, National Geodetic Survey, National Oceanic and Atmospheric Administration, in providing KARS software, the associated consultations, field work assistance, and sharing the Holland West tide gauge data. I particularly would like to thank Dr. Michael E. Parke, who conducted Lake Michigan GPS Buoy Campaign, for the help in processing GPS buoy data for this research. Dr. Yi and Mr. Kyle Snow's help in providing TOPEX/POSEIDON data and GPS geodetic network result of the campaign is acknowledged. In addition, Also, I thank Joktan Kwiatkowski for reviewing the grammar of this report.

Finally, I would like to express my deepest gratitude and appreciation to my parents, family members and dear wife Yu-yun Lin for their love, encouragement and sacrifices during my study at the Ohio State University.

# Table of Contents

ABSTRACT ..... iii
PREFACE ..... v
ACKNOWLEDGMENT ..... vii
1. INTRODUCTION ..... 1
1.1 Satellite Radar Altimetry ..... 2
1.2 Buoy Water Level Measurement System ..... 5
1.3 Tide Gauges ..... 6
1.4 Summary ..... 7
2. RADAR ALTIMETRY SYSTEM OVERVIEW ..... 9
2.1 Radar Altimeter Mission Description ..... 9
2.2 Altimeter Measurements ..... 11
2.3 Corrections ..... 13
3. RADAR ALTIMETRY ABSOLUTE CALIBRATION ..... 19
3.1 Closure ..... 19
3.2 In Situ Data Sets ..... 22
3.2.1 DGPS Buoy ..... 22
3.2.2 Tide Gauges ..... 24
3.3 Geoid Gradient ..... 27
3.3.1 Geoid Gradient Modeled with Bins ..... 27
3.3.2 Geoid Gradient Modeled with Geostatistical Approaches ..... 28
4. LAKE MICHIGAN CAMPAIGN AND DATA ANALYSIS ..... 33
4.1 Lake Michigan Campaign ..... 33
4.2 Altimeter-Derived Water Levels ..... 37
4.3 GPS-Derived Water Levels ..... 44
4.4 Error Budget of Altimeter Bias Estimated with GPS Buoy Data ..... 47
4.5 Error Budget of Altimeter Bias Estimated with Tide Gauge Data ..... 49
4.6 Summary ..... 55
5. CONCLUSION ..... 57
REFERENCES ..... 59
APPENDIX A ..... 63
APPENDIX B ..... 67

# CHAPTER 1

# INTRODUCTION

Recent studies of using long-term island and coastal tide gauges (about 100 years) indicate that the global sea level rise is at a rate of 1.8 to 1.9 ± 0.1 mm/year (e.g., Douglas 1997, 1991; Trupin and Wahr, 1990; Warrick and Oerlemans, 1990). The global sea level rise has drawn public attention since the global sea level has risen about 20 cm since 1990, as indicated by the studies. This effect is critical to human and social well being. It is therefore critical to accurately measure global sea level change using different and complementary techniques. For example, tide gauges and, more recently, satellite radar altimetry have been used to collect sea level height measurements; however, both have their own disadvantages.

Tide gauges have been used for centuries to collect sea level measurements with respect to the local vertical benchmarks, which do not always refer to the geocentric system or have errors. The use of tide gauges in global mean sea level studies is also limited by the inability of modeling or measuring vertical motions of the benchmarks on the solid earth to which the tide gauge sea level measurements are referred. Examples of the vertical motions include the Glacial Isostatic Adjustment (GIA) (e.g., Peltier, 1996) of the solid earth causing a change of topographic height and to a lesser extent, geoid change. There may also be vertical motion due to episodic movements, such as tectonic motions and earthquakes. These movements and their locations affect the benchmark and they need to be correctly surveyed or modeled in order to maintain the consistency of the tide gauge data.

On the other hand, satellite radar altimetry is able to provide global coverage (±81.5° latitude) of the sea level measurements with an accuracy of a few centimeters. Unlike tide gauges, satellite radar altimeters directly 'measure' instantaneous sea surface height (ssh), the ellipsoidal height of the instantaneous sea surface above a specified reference ellipsoid, in an absolute sense. With simultaneously operating satellite altimeters (TOPEX/POSEIDON, European Remote Sensing Satellite-2 and Geosat Follow-On) and future missions (e.g., Jason, ENVIironment SATellite and National Polar-orbiting Operational Environmental Satellite System), decadal or longer accurate observations of the global mean ssh are anticipated. These measurements are invaluable for the studies of long-term global sea level change. However, the use of satellite radar altimetry in global mean sea level studies is mostly limited by inadequate knowledge of the bias and drift of each individual altimeter system, which need to be measured or calibrated. Other factors also limit its use in global mean sea level studies, such as its relative short data span (about 15 years since Geosat) compared with the tide gauge data span, complexity in instrumental, media and geophysical corrections, as well as the potential sampling error associated with its spatial and temporal resolutions (Urban, 2000; Guman, 1997). In general, those corrections are in the order of few mm per year, the same or larger

than the signal of the sea level change, that increase the difficulties of using altimeters for the global sea level monitoring (Shum et al., 1999). However, the dominant error source remains to be the inadequate knowledge of the altimeter bias and drift (Urban, 2000).

The objective of this study focuses on the study of processes for the accurate determination of the bias and the drift of each individual altimeter system. The technique of the radar altimeter absolute calibration will be studied by comparing the altimeter-observed ssh with the in situ data observed independently by the GPS buoy and tide gauges. In March of 1999, a GPS buoy campaign was conducted in Lake Michigan for calibration of the TOPEX/POSEIDON Side B (TSB) altimeter and the Geosat Fallow-On (GFO) altimeter by the Laboratory for Space Geodesy and Remote Sensing Research of the Department of Civil and Environmental Engineering and Geodetic Science at the Ohio State University in cooperation with the National Geodetic Survey, National Oceanic and Atmospheric Administrations. The lake was chosen in this campaign because of the relatively calm water conditions such as waves and wind compared with those in the ocean. Lake level height measurements from the GPS buoy and from the Holland West tide gauge were collected as the in situ data sets. The results are expected to be in line with other calibration stations.

## 1.1 Satellite Radar Altimetry

Satellite radar altimetry is a revolutionary technology in oceanography to synoptically map the global ocean's surface. It is able to observe global oceanic phenomena with unprecedented accuracy (e.g., several centimeters in ssh). Its temporal resolution is 1-2 weeks and spatial resolution is about 50 km. One of the first discussions of using satellites to observe ssh was at the 1969 Williamstown Conference of Solid Earth and Ocean Physics (Kaula, 1969). Since then, there are a number of altimeter missions flown and scientific results of these missions have been published. Table 1.1 presents a list of past and future altimeter missions and orbital parameters.

The measuring principle of satellite radar altimetry is relatively straightforward. It sends out an electromagnetic radar pulse and calculates the time it takes when the radar signal is bounced back by the water surface of the earth and received by the sensor. The actual around-trip travel time of the radar pulse is precisely recorded by the on-board clock (Ultra Stable Oscillator). Radar altimetry is exclusively designed to be used over the oceans and large inland lakes because of the favorable reflectivity of the radar signals over the water body. By multiplying the one-way travel time with the speed of light; the range between the satellite to the instantaneous water surface can be determined. Also, the ellipsoidal height of the instantaneous water surface can be determined by using the ellipsoidal height of the spacecraft

obtained from a number of satellite tracking techniques.. The geometry of this measuring principle will be further explained in Chapter 2.

There are three fundamental measurements of a satellite radar altimeter: the instantaneous range, the wave height and the wind speed. They are inferred from the waveform analysis. In addition, there are several corrections, categorized into instrumental, media and geophysical corrections, which need to be applied to the raw altimeter measurements before utilizing them. The details about waveform analysis and corrections will be discussed in Chapter 2.

As is common for electronic or radar instruments, the radar altimeter may deviate from the true range by a systematic error. It is called the altimeter bias, which is indeed a systematic mis-closure to the true measurement (Christensen et al., 1994). This instrument can be calibrated by providing the accurate ground truth. Since the true ssh is unavailable, accurate in situ ssh data sets are considered as the alternative. There are several calibration stations that have been established worldwide; for example, Harvest Platform (Christensen et al., 1994), Burnie site (White et al., 1994) and Lampedusa Island (Menard et al., 1994). They measure the sea level independently using tide gauges and the associated media and geophysical corrections providing accurate in situ ssh data to compare with altimeter-observed ssh. The procedure is called radar altimeter absolute calibration (Kruizinga, 1997; Christensen et al., 1994).

| Mission | Active Dates (month/year) | Altitude (km) | Inclination (degrees) | Repeat Period (days) | Agency |
|---|---|---|---|---|---|
| GEOS-3 | 4/75 – 12/78 | 840 | 115 | Non-repeat | NASA |
| SEASAT (17-day repeat) | 7/78 – 9/78 | 790 | 108 | 17 | NASA |
| SEASAT (3-day repeat) | 9/78 – 10/78 | | | 3 | NASA |
| GEOSAT GM | 3/85 – 11/86 | 780 | 108 | Non-repeat | US Navy |
| GEOSAT ERM | 11/86 – 12/89 | | | 17 | |
| ERS-1 A | 7/91 – 11/91 | 785 | 98.5 | 3 | ESA |
| ERS-1 B | 11/91 - 3/92 | | | 3 | |
| ERS-1 C | 4/92 – 12/93 | | | 35 | |
| ERS-1 D | 12/93 - 4/94 | | | 3 | |
| ERS-1 E | 4/94 - 9/94 | | | 168 | |
| ERS-1 F | 9/94 - 3/95 | | | 168 | |
| ERS-1 G | 4/95 - 6/96 | | | 35 | |
| TOPEX/POSEIDON | 8/92 – present | 1354 | 66 | 10 | NASA CNES |
| ERS-2 | 4/95 – present | 785 | 98.5 | 35 | ESA |
| GFO-1 | 5/98 – present | 800 | 108 | 17 | US Navy |
| ENVISAT-1 | 2001 | 785 | 98.5 | 35 | ESA |
| JASON-1 | 2001 | 1354 | 66 | 10 | NASA CNES |
| NPOESS* | 2006* | 800-1300* | 66-98.5* | 10-35* | Int'l |

Table 1.1: Satellite altimeter missions and orbital parameters (* planned).

## 1.2 Buoy Water Level Measurement System

Figure 1.1: GPS satellite constellation (Courtesy of R. Rummel).

The NAVSTAR GPS (NAVigation System with Time And Ranging Global Positioning System) is a satellite-based radio navigation system providing precise three-dimensional position, navigation and time information to suitably equipped users. It will be continuously available on a worldwide basis, and is independent of meteorological conditions. Although it was originally designed for the military purposes, its civilian applications keep increasing. The complete GPS system consists of 24 operational satellites providing 24-hour, all-weather navigation and surveying capability worldwide. Figure 1.1 presents the final GPS constellation: 24 satellites are distributed in six orbital planes, which are evenly spaced in right ascension and are inclined by 55° with respected to the equator. The orbital altitudes of orbits are 20,200 km above the earth so that there are at least four satellites available simultaneously above the horizon anywhere on the earth, 24 hours a day (Leick, 1995; Seeber, 1993).

Codes (pseudoranges) and carrier phases are two major observables in GPS positioning. With two receivers (one corresponding to the reference station whose coordinates are precisely known, whereas the other refers to the rover to be determined) taking data simultaneously, the common errors such as the clock synchronization errors and similar tropospheric delays can be canceled out at both stations. It is known as the relative GPS positioning, which increases the relative accuracy dramatically. However, this, in general, requires post-processing the data. Differential GPS (DGPS) is a method, which the data is

processed in real-time and the corrections are transmitted from thereference station to the rover (or vise versa). These technologies have been exclusively used in different fields such as navigation, geodesy and surveying with accuracy 0.5 cm ± 1 part per million of the baseline length (Seeber, 1993).

A GPS buoy is equipped with a geodetic GPS receiver and an antenna on top of it. Along with another receiver occupied at the reference station, where the geocentric coordinates are precisely known, the positions of the buoy can be determined by GPS relative positioning. Although DGPS is also possible in determining buoy locations, it subjects to the availability of the radio transmission. A GPS buoy, with an accurate reference station within the suitable range, is able to provide the three-dimensional coordinates of the instantaneous sea surface in the geocentric reference frames such as WGS 84 (World Geodetic System) or ITRF (International Terrestrial Reference Frame). It, in a way, measures the mean ssh by averaging the high-frequency signals such as wave motions and systematic noise. There are two main designs (waverider and spar) that have been historically used in radar altimeter absolute calibrations (c.f., Kruizinga, 1997; Schutz et al., 1995; Born et al., 1994; Hein, 1992; Rocken et al., 1990). For example, Hein (1992) measured the geocentric coordinates of the instantaneous sea surface with phase observations collected by a spar buoy in a 0.5-sec sampling rate and claimed that the accuracy was in the centimeter level. Section 3.2.1 will discuss the designs, current hardware and software limitation, and data processing in addition to the errors associated with the GPS buoy.

In summary, GPS buoys provide a convenient and accurate tool, especially with the lightweight waverider design, to directly measure the instantaneous sea surface height in the geocentric terrestrial reference system. This ability enables many diverse potential applications to become important instruments in calibrating satellite radar altimeters.

## 1.3 Tide Gauges

Tide gauges are generally located in coastal regions and near islands. They measure the sea surface change with respect to the local vertical benchmarks. Errors resulting from the inability to model or measure vertical motions of the benchmarks on the solid earth (to which the tide gauge water levels refer) certainly limit the possibility of directly comparing tide gauge levels with altimeter ssh (Shum et al., 1999). Also, the height system that tide gauge measurements refer to may vary. It could be the orthometric height above the geoid, or mean sea level, along the curved plumb line (Heiskanen and Moritz, 1987). It could also be the dynamic height (geopotential number divided by the normal gravity at standard latitude), which is usually at 45° (Heiskanen and Moritz, 1987). Since the horizontal and vertical datums are

commonly treated separately, both of the height systems mentioned above are not consistent with the ellipsoidal, geocentric height that altimeter-observed ssh refer to. Hence, height conversion from various height systems to the ellipsoidal one is necessary prior to using tide gauge ssh measurements as the in situ data for radar altimeter absolute calibration.

Tide gauges nevertheless produce a continuous, long-term (decadal or longer) sea level history that can be used to verify the long-term low-frequency ssh drift provided by altimeters (Mitchum, 1996). However, there are only a few tide gauges on the earth that are passed exactly (within 1-2 km) by altimeter ground tracks. Some of them are located at the end of an altimeter ground track where the altimeter ssh measurements might be problematic. Therefore, it is necessary to consider a geoid or mean sea surface gradient, which is the height difference between the locations of the tide gauge and the desired altimeter sub-satellite point. It is also necessary to consider time variation effects. Auxiliary ssh measurements are required to construct a geoid gradient model, in order to translate the location of the tide gauge to where good altimeter ssh measurements are. A detail of using the geostatistical approach such as kriging will be discussed in Chapter 3.

.

## 1.4 Summary

Both GPS buoys and tide gauges demonstrate the ability of providing in situ data sets for radar altimeter absolute calibrations, although some technical issues exist. They can potentially help in constructing the accurate long-term global ssh measurements, which assist in studies and researches of the sea level change.

A radar altimetry mission description and the system overview will be discussed in Chapter 2. Chapter 3 describes the so-called closure equation and technical issues such as the data processing and the construction of a geoid gradient model with the geostatistical approach. Chapter 4 presents the result of T/P absolute calibrations with the data from a cooperative campaign conducted by the Laboratory for Space Geodesy and Remote Sensing Research at the Ohio State University and the National Geodetic Survey, National Oceanic and Atmospheric Administration (NGS/NOAA), in Holland, Michigan in 1999. Finally, Chapter 5 summarizes the study. Lake Michigan Altimeter Calibration Campaign work logs and the list of acronyms can be found in Appendix A and Appendix B.

# CHAPTER 2

## RADAR ALTIMETRY SYSTEM OVERVIEW

## 2.1 Radar Altimeter Mission Description

Satellite altimeter missions are currently operating (T/P, ERS-2 and GFO) and anticipated to be abundant in the next decade including Jason, Envisat and NPOESS. All these instruments are anticipated to contribute to the measurements of the global mean sea level change. Therefore, the monitoring and calibrations of the biases and drifts of these altimeter systems are required. This section provides a description of an example radar altimeter system: T/P. It is a joint radar altimetric satellite mission by National Aeronautics and Space Administration (NASA), USA and Centre National d'Etudes Spatiales (CNES), France. It was launched on August 10, 1992 with an approximate 10-day repeat circular orbit, 66° inclination, and an altitude of 1354 km. It was the first radar altimetric mission specifically designed for studying general ocean circulations (Fu et al., 1994) and therefore strict accuracy is required. The mission design was innovated many times to meet these requirements. They include the first dual frequency (C- and Ku-band) altimeter for the first order ionospheric delay corrections, a three-channel microwave radiometer for measuring integrated water vapor contents, and three satellite tracking systems including Satellite Laser Ranging (SLR), Doppler Orbitography by Radiopositioning Integrated on Satellite (DORIS) and GPS for precise orbit determination. T/P measures sea surface height with a 1.7-cm precision and an overall accuracy of 4.7 cm. This accuracy is 2 times better than the original mission requirement of 13.4 cm (Fu et al., 1994).

The TOPEX altimeter has redundant A and B hardware. Data from TOPEX Side A (TSA) began to show performance degradation. Therefore, after 6 years of exclusive Side A operation, the TOPEX Science Working Team and the Jet Propulsion Laboratory engineers decided to evaluate the performance of Side B. Since 15:04 UTC on February 10, 1999, TOPEX Side B (TSB) has been switched on for future operation (TOPEX Team, 2000; Hayne and Hancock, 2000). The success of the T/P mission has ensured the place of satellite oceanography as both a prominent and bountiful area of scientific study (Urban, 2000).

The primary objectives of this study include the use GPS-buoys and tide gauges as the in situ data sets for TSA and TSB absolute calibration in an attempt to potentially improve the accuracy of the long-term (decadal or longer) global ssh measurements. Based upon the experience and knowledge obtained from this study, it expectantly provides a generic

technology about the satellite radar altimeter absolute calibration using GPS buoy and tide gauges measurements.

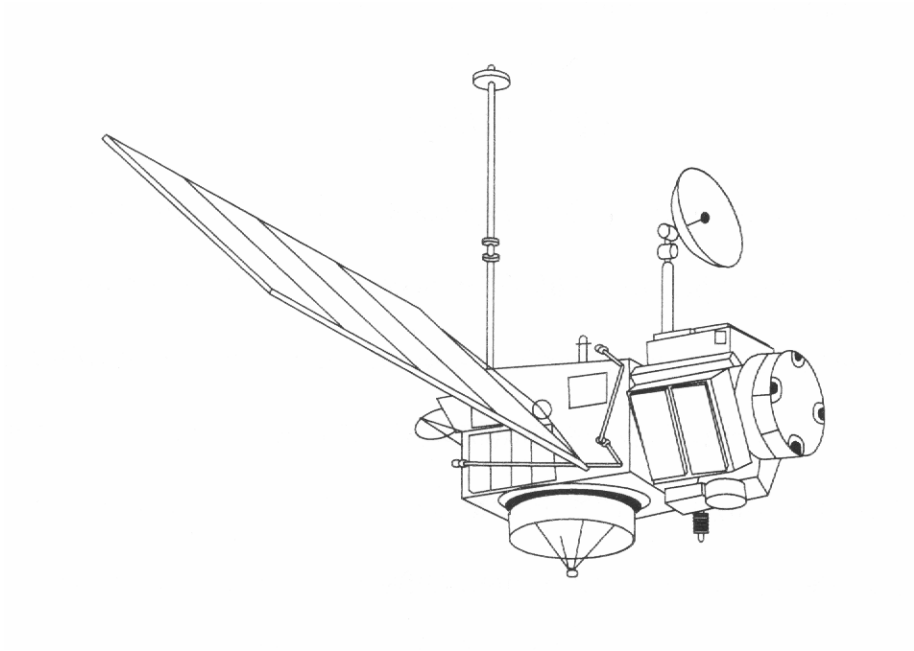

Figure 2.1: TOPEX/POSEIDON spacecraft.

## 2.2 Altimeter Measurements

The radar altimeter emits a radar pulse and measures its travel time when the radar pulse is bounced back to the satellite by the instantaneous sea surface. As a result, the observable in satellite radar altimetry is actually a time series of the received power distribution of the reflected pulses, which is often referred to as the altimeter waveform. Figure 2.2 presents an ideal average altimeter waveform for water surface and its associated surface illumination pattern. Due to favorable water reflectivity, radar altimetry is designed to be primarily used over the oceans and large inland lakes although measurements over reflected surfaces such as ice sheets and lands have contributed to scientific studies.

As illustrated in Figure 2.2, $t_R$ represents the time at the half power point, which is determined at half of the maximum received radar power and represents the one-way travel time of the pulse. By multiplying it with the speed of light, the range between the satellite radar antenna to the instantaneous sea surface can be determined. It is one of the fundamental altimeter measurements. The wave height on the sea surface affects the waveform slope in the leading edge, which is referred to as the significant wave height (SWH). In addition, the wind changes the waveform slope in the trailing edge. It is called back scattering cross section ($s_0$) at nadir represented by the slope of the trailing edge of the waveform. Therefore, the altimeter range, SWH, and $s_0$ are three fundamental altimeter measurements that can be derived from the altimeter waveform. $s_0$ can be converted to the non-directional wind speed using model function.

AGC (Automatic Gain Control) is the maximum returned energy of an altimeter waveform. It is often used to normalize the altimeter waveform when sensing different surfaces such as land, ocean and ice. Since this study focuses on the bias and drift determinations, only altimeter range over water will be directly discussed although both SWH and $s_0$ affect the ssh measurements in the form of sea state bias correction.

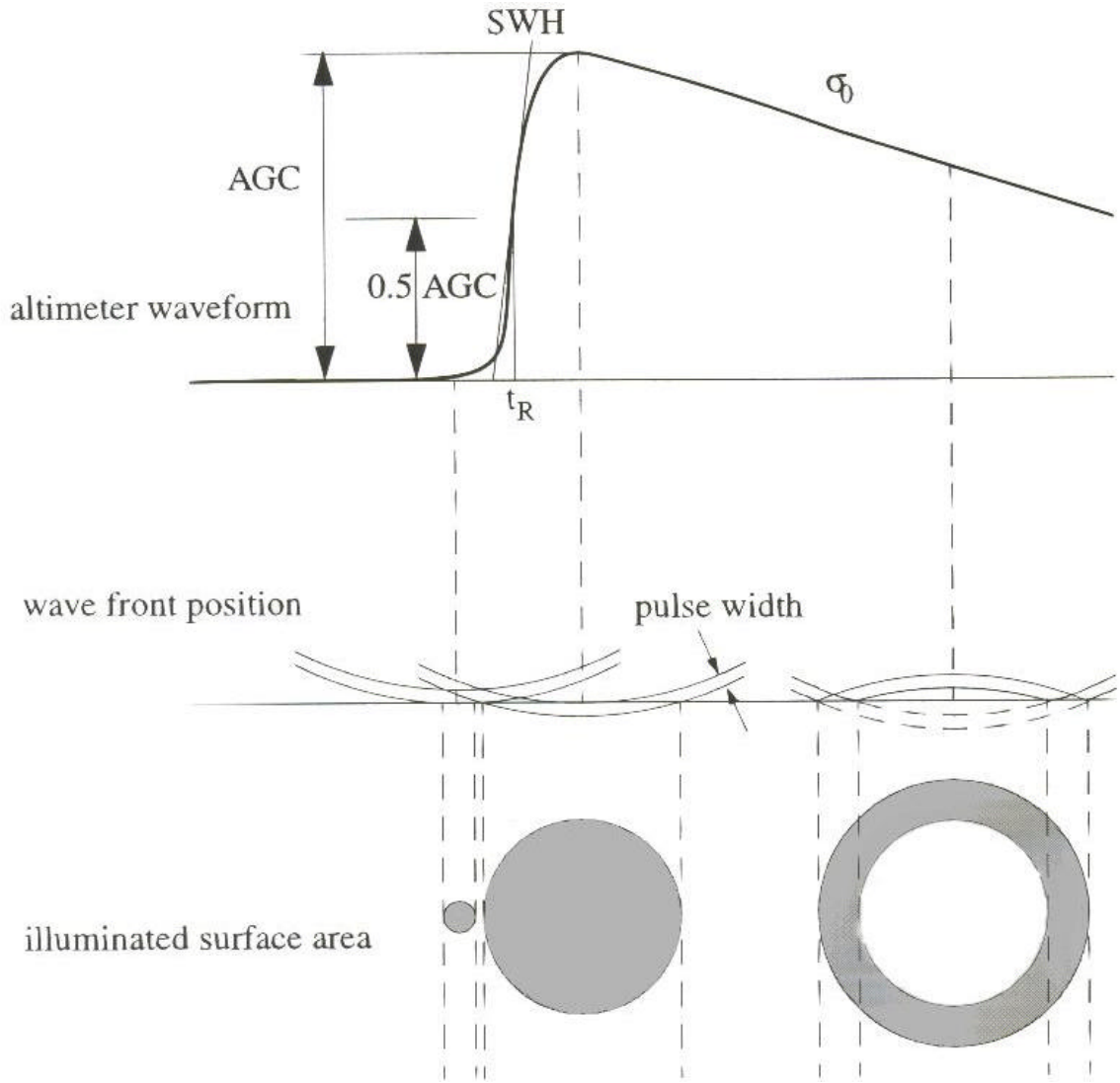


Figure 2.2: The ideal average altimeter waveform for the water and its illumination pattern (Kruizinga, 1997).

## 2.3 Corrections

Figure 2.3 presents the geometry of satellite altimetry in an ideal case. Assuming all quantities are normal to the reference ellipsoid, the instantaneous ssh, which is the geocentric height above the selected reference ellipsoid can be formulated as (2.1).

$$h_{ssh} = h_{orbit} - h_{altcor} \tag{2.1}$$

$\boldsymbol{h_{ssh}}$ is the instantaneous sea surface height. $\boldsymbol{h_{orbit}}$ is the altitude of computed satellite orbit determined by different satellite tracking techniques such as SLR, DORIS and GPS. The deviation of the computed satellite orbit from the true orbit is mainly caused by the error in the terrestrial gravity field (often force models) used in orbit determination, errors in the ground tracking stations, measurement errors, and the imperfection of the orbit computation procedure (Seeber, 1993). $\boldsymbol{h_{altcor}}$ is the corrected altimeter range (will be discussed later).

Instantaneous sea surface height ($\boldsymbol{h_{ssh}}$) may be considered as the fundamental measurement and it is realized as the geocentric (or ellipsoidal) height of the instantaneous sea surface. The deviation of the instantaneous sea surface from the geoid can be split into the mean dynamic ocean topography, a secular quantity, and the time-varying dynamic ocean topography, which is caused mainly by time-varying phenomena such as tides, currents and atmospheric loading etc. The total effect of both is about 1 to 2 meters and is considered as the sea surface topography (sst), which is the difference between the geoid and the mean sea surface. The further descriptions about sea surface topography can be found in Calman (1987).

Usually the mean sea level, which is called the stationary sea surface by Lizitzen (1974), is understood to be the sea surface that is free from all time-dependent variations such as tides, currents and atmospheric pressure. However, the sea surface is not stationary and it deviates from the geoid by a mean sea surface topography and a time-varying variation. Hence, the commonly used approximation of the geoid by the mean sea surface is not valid in this case, if a resolution of better than 2 m is required (Seeber, 1993).

The altimeter range, which is derived from the multiplication of a half of the travel time (i.e., $t_R$ in Figure 2.2) and the speed of light, does not really represent the true range between the instantaneous sea surface and the satellite. Altimeter range corrections are

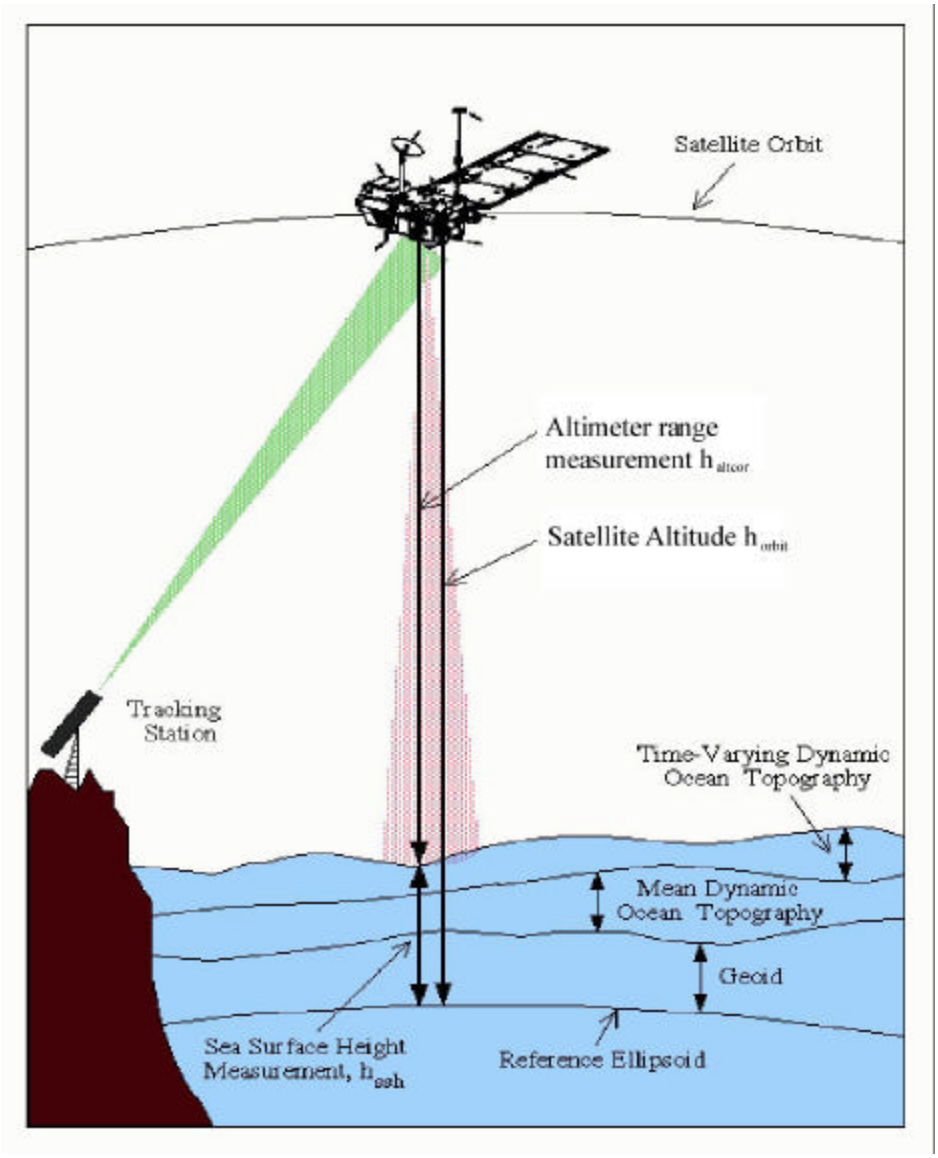


Figure 2.3: The geometry of satellite radar altimetry.

are necessary whose fidelity directly affects the accuracy of the corrected altimeter range, and hence, measured ssh. There are three categories of altimeter range corrections: instrumental, media, and geophysical. They need to be applied to the altimeter range measurements so that the corrected ssh can better represent the true ssh. However, all the corrections are either measured (e.g., ionosphere and wet troposphere) or empirical modeled. Therefore, individual correction in the form of biases and drifts could manifest as part of the total altimetric bias and drift.

(1) Instrument Corrections.

These corrections are necessary due to the variations in spacecraft hardware resulting from the nature of the return signal, satellite motion and pointing errors, satellite temperature variations, and other hardware properties. They include, among others, Doppler corrections, center-of-mass offsets, mispointing tracking adjustments, and internal calibrations. The Doppler correction corrects the range measurements to account for Doppler shift due to the velocity of the satellite. The center-of-mass corrections correct the phase center of the radar altimeter antenna to the center of mass of the spacecraft, from which the orbit is computed. The internal calibration, for example on T/P, is a measured range drift due to the changes in the internal electronic path delay. This internal instrument drift, or the Wallops Correction, is derived by NASA/Wallops and is reported monthly (Hayne, 1999).

The Sea State Bias (SSB) is another important correction including the effects of the electromagnetic bias, skewness bias, and tracker bias (Gaspar, 1994). It is required because the troughs of waves reflect the microwave pulses better than the crests. This causes the altimeter range measurement to be biased towards the troughs (i.e., measured range appears longer than the true range).

(2) Media Corrections

These corrections are necessary because the radar pulses are slow down while passing through atmosphere. This effect results in a longer altimeter range (or shorter ssh measurement). Air, water vapor, and free electrons are three main components in the atmosphere that slow down the radar beam. The high variability of atmospheric water vapor and electron density makes accurate determination of corrections difficult (Urban, 2000). Media corrections include ionospheric delay, dry tropospheric delay, and wet tropospheric delay.

Ionospheric delay is frequency-dependent; for example, the ionospheric delay in 14 GHz (Ku-band) is about 5 cm to 20 cm, depending on the level of ionization (Lorell et al., 1982). However, it can be eliminated with the linear combination of the range measurement in different frequencies. For example, T/P is equipped with a dual-frequency (C- and Ku-bands)

altimeter and it uses the returned signal from both frequencies to calculate the first order ionospheric delay.

Tropospheric delays are radar frequency independent. Dry tropospheric delay is caused by the dry-air component in the atmosphere, which cannot be directly measured by sensors on altimeter satellites. Hence, the operational atmospheric global circulation models (AGCM), which provide global sea surface pressure data, are required to interpolate the dry-air component to the space-time coordinates of each range measurement and to compute the delay using a physical model. The average dry tropospheric delay is about 2.3 m (Tapley et al., 1982).

Wet tropospheric delay (or water vapor path delay) is caused by the water vapor contents in the atmosphere, which can be modeled by AGCM or can be directly measured by an on board microwave radiometer. All present and proposed radar altimeter satellites include onboard active microwave radiometers to measure the water vapor along the nadir path. However, the water vapor contents measured by a radiometer could be corrupted by the liquid water along the path (e.g., cloud or rain). Also, current microwave radiometers have much larger footprints than the radar altimeter; as a consequence, the non-ocean surfaces within the footprint (e.g., coastal lands and ice) will thwart the radiometer from getting accurate water vapor contents. Therefore radiometer-measured tropospheric delays near the coast are problematic. This is the reason for which altimeter ssh measurements are less accurate near the coasts. AGCM model-computed delays, in this case, could be used in place of radiometer-measured delays.

(3) Geophysical Corrections

Geophysical corrections include tides (solid earth tide, ocean tide, and pole tide) and the inverted barometer (IB) correction. The inverted barometer effect describes the ocean surface deformations due to atmospheric loading (Ponte, 1993). The sea level is reduced 1 cm with an approximately 1-mbar additional atmospheric pressure difference. For example, Dorandeu and Le Tron (1999) provide further information on IB correction.

With all corrections applied, the corrected altimeter range in (2.1) can be computed as following.

$$h_{altcor} = (h_{alt} + h_{instru} + h_{ssb} + h_{dry} + h_{wet} + h_{iono} + h_{tides} + h_{ib}) - b - e \qquad (2.2)$$

where

$\boldsymbol{h_{altcor}}$ is the corrected altimeter range,

$\boldsymbol{h_{alt}}$ is the raw altimeter range, derived from the multiplication of half of the travel time with the speed of light,
$\boldsymbol{h_{instru}}$ is the total of the instrument corrections,
$\boldsymbol{h_{ssb}}$ is the sea state bias correction,
$\boldsymbol{h_{dry}}$ is the dry tropospheric delay,
$\boldsymbol{h_{wet}}$ is the wet tropospheric delay,
$\boldsymbol{h_{iono}}$ is the ionospheric delay,
$\boldsymbol{h_{tides}}$ is the tides corrections including solid earth tide, ocean tide, and pole tide,
$\boldsymbol{h_{ib}}$ is the inverted barometer correction,
$b$ is the altimeter bias, and,
$\boldsymbol{e}$ is the composite random noise.

By inserted (2.2) into (2.1), the mean sea surface height can be derived by (2.3).

$$h_{ssh} = (h_{orbit} - h_{alt} - h_{insru} - h_{ssb} - h_{dry} - h_{wet} - h_{iono} - h_{tides} - h_{ib}) + b + e \tag{2.3}$$

The terms in parentheses are hopefully to represent the mean ssh at the sub-satellite point better than the one derived merely from the raw altimeter range. The mean ssh measurement deviates from this quasi-true one with an altimeter bias and a composite random noise. This is, as mentioned before, called altimeter range bias, which is a closure between the true ssh and the altimeter-measured one. It is of importance for acquiring the accurate ssh measurements, especially in linking multiple satellite radar altimeter missions. Again, all corrections mentioned above are based on other measurements and/or computed based on physical model. Unknown systematic errors and the random error in each individual correction contribute, at least in part, to the altimeter bias and the composite random error in (2.3). One possible way to resolve the altimeter bias is by comparing the ground truth with the altimeter ssh measurements. This approach is called radar altimeter absolute calibration. Chapter 3 discusses radar altimeter absolute calibration techniques. The T/P calibration results using GPS buoy data and the Holland West tide gauge historical ssh record in Lake Michigan Campaign are reported in Chapter 4.

# CHAPTER 3

## RADAR ALTIMETRY ABSOLUTE CALIBRATION

### 3.1 Closure

Altimeter bias is defined as the difference between the altimeter sea surface height (ssh) measurement and the "true measurement". The bias is caused by instrument imperfection, errors in each individual correction, and other possible random/systematical errors relevant to the altimeter and the corrections. The combined error causes the altimeter ssh measurement to deviate from the truth. As mentioned in Chapter 2, radar altimeter absolute calibration is one way to resolve altimeter bias by providing the ground truth coincident with altimeter ssh measurements. The ground truth will be referred to as the in situ data sets, which are precise measurements collected by other instruments such as GPS buoys or tide gauges. They are independent to altimeter ssh measurement and therefore can be used as the in situ data sets for radar altimeter absolute calibration.

The accuracy of the sea level variation is about 1 cm and therefore the required accuracy of altimeter bias and drift estimations should also be in the comparable

magnitude. The current required accuracy for altimeter bias and drift is 1 cm and less than 1 mm per year respectively. The altimeter bias and its drift can be estimated by comparing altimeter ssh measurements with the in situ data sets over the mission lifetime (several years to decadal). In this sense, the altimeter bias becomes the closure between altimeter ssh measurement and the selected technique that provides the in situ data. Christensen et al. (1994) pointed out that referring the closure as altimeter bias is a misnomer because the closure is contributed by both altimeter and in situ measurements. We call the closure the altimeter bias only for the sake of brevity and for consistency with tradition.

At each calibration site for every altimeter overflight there exists the following condition:

$$h_a - h_i = b + \Delta t \cdot d(\Delta t) + e, \qquad e \sim (0, \Sigma) \tag{3.1}$$

where $\boldsymbol{h_a}$ is the altimeter ssh measurement with all corrections applied (as described in Section 2.3), $\boldsymbol{h_i}$ denotes the in situ sea surface data measured independently, $D\boldsymbol{t}$ is elapsed time from the beginning of the altimeter operation, $\boldsymbol{e}$ is composite random error with a zero mean and a variance of $S$, $b$ and $d(D\boldsymbol{t})$ are altimeter bias and drift to be estimated. Although $d(D\boldsymbol{t})$ is a function of time, it is treated as a linear drift in this study. In other words, the drift is assumed fixed in the whole altimeter mission. Equation (3.1) can therefore be revised as the following form:

$$h_a - h_i = b + \Delta t \cdot d + e, \qquad e \sim (0, \Sigma) \tag{3.2}$$

$b$ and $d$ are non-random parameters and $e$ is a stochastic variable. They are unknowns in Equation (3.2) and cannot be solved with only one single closure equation. Apparently, more closure equations are necessary to be collected in order to solve for altimeter bias and drift with least squares. However, the annual and semi-annual signals (which are two dominant signals found in altimeter ssh measurements) need to be accounted for. Hence, Equation (3.2) can be revised as (3.3) (Kruizinga, 1997).

$$\begin{aligned} h_a - h_i = b + \Delta t \cdot d &+ C_1 \cos(w_1 \cdot \Delta t) + S_1 \sin(w_1 \cdot \Delta t) \\ &+ C_2 \cos(w_2 \cdot \Delta t) + S_2 \sin(w_2 \cdot \Delta t) \\ &+ \mathrm{e} \end{aligned} \tag{3.3}$$

$$w_1 = \frac{2p}{365}$$

$$w_2 = \frac{4p}{365}$$

$\boldsymbol{C_1}$, $\boldsymbol{C_2}$, $\boldsymbol{S_1}$ and $\boldsymbol{S_2}$ are harmonic constants with $w_{\boldsymbol{1}}$ and $w_{\boldsymbol{2}}$ being annual and semi-annual frequencies respectively. $b$, $d$, $\boldsymbol{C_1}$, $\boldsymbol{C_2}$, $\boldsymbol{S_1}$ and $\boldsymbol{S_2}$ are unknown parameters to be determined with the observations being the difference between the altimeter ssh measurements and the in situ data set. If both $\boldsymbol{h_a}$ and $\boldsymbol{h_i}$ were perfectly measured, the annual- and semi-annual signals would be removed and only $b$ and $d$ could be left. Equation (3.3) needs to be

solved with least squares as well. It is anticipated that more redundant measurements of closure equations, or calibration samples, established at a single calibration site will improve the accuracy of bias and drift determinations through averaging down of the random error. In addition, the unknown parameters (altimeter bias, drift, and signals) are the same for one individual altimeter at other calibration sites as well. Therefore, it is anticipated that more calibration sites involved in the closure process would help improve the accuracy of bias and drift estimation; at least to reduce the impact of the random errors involved in the calibration.

Although both altimeter ssh measurements and the in situ data are expected to be taken simultaneously when the satellite overflies, both data sets are not synchronized. The time of closest approach (tca) is consequently considered to be the reference epoch. Both altimeter ssh measurements and the in situ data require interpolating and then are compared to each other at the reference epoch (i.e., tca). For example, 10-Hz Topex altimeter measurements can be used, instead of using 1-Hz data, in order to provide sufficient data for interpolation. In order to eliminate the random noise in both systems, a low-pass filtering will be performed.

In some cases, the in situ data (e.g., tide gauges) may not be exactly located on the sub-satellite points where altimeter ssh measurements are taken. It is necessary to account for the geoid gradient (more correctly, known as mean sea surface gradient) that is the sea surface height change due to measurements made at different locations. By applying the geoid gradient (it will be discussed in Section 3.3) to either $\boldsymbol{h_a}$ or $\boldsymbol{h_i}$, the ssh measurements at different places are "translocated" to the same point and will be compared with each other. However, adding one more correction to the closure equation increases the estimation errors in $b$, and $d$; especially the geoid gradient, which often dominates other error sources in bias/drift determinations. Hence, it should be avoided if possible.

## 3.2 In Situ Data Sets

### 3.2.1 DGPS Buoy

A Differential GPS (DGPS) buoy is deployed on the water surface and collects the GPS phase and/or code observations to measure the water surface change in the kinematic mode with the sampling rate up to 0.5 seconds. It can reach the accuracy of a few centimeters (e.g., Born et al., 1994; Hein et al., 1992; Rocken et al., 1990). Historically there are two basic buoy designs used in altimeter calibrations (spar and floater, as illustrated in Figure 3.1). Rocken et al. (1990) tested the feasibility of the precise sea level measurements with a floater buoy in Scripps pier at La Jolla, California. Hein et al. (1992) and Born et al. (1994) used the spar buoys in the North Sea for ERS-1 and at Harvest for T/P calibration respectively. Schutz et al. (1995) and Kruizinga (1997) used a waverider buoy (a floater design) in Galveston Bay for T/P calibrations. There are on-going projects conducted by NOAA/NGS (National Oceanic and Atmospheric Administration, National Geodetic Survey) in the San Francisco Bay and Chesapeake Bay off the coast of Baltimore. They tested an autonomous spar buoy in an attempt to observe the sea level boundary conditions for regional circulation forecast and modeling (Zilkoski et al., 1996). Although these two designs are commonly seen in the previous altimeter calibrations, other designs may be employed.

A GPS waverider buoy that was used in this study is built by attaching a high quality choke ring antenna (to reduce the multipath) on a floater buoy. Phase and code observations are recorded in the kinematic mode and the buoy positions are determined on the epoch-by-epoch sense. GPS data can be processed in the real-time mode (if the radio transmission equipment is available) or can be post-processed with respect to the reference stations near by the shore. A waverider buoy freely floats on the water surface. Since the period of waves is normally around 2-20 seconds per cycle in deep water (deeper than 200 m) and much shorter in the shallow water, high GPS sampling rate is required. To prevent it from the aliasing, Born et al. (1994) suggested the 1-Hz sampling rate for a waverider buoy in the general cases. However, Kelecy et al. (1994) have shown that these two different designs give equivalent sea level measurements.

Figure 3.1: A waverider buoy (left, a floater design). An autonomous spar buoy (right) used by NOAA/NGS in San Francisco Bay (Zilkoski et al., 1996).

A spar buoy, on the other hand, is designed to eliminate the buoy movement with the stabilizing fins and ballast underneath the water. The high-frequency signals (e.g., random errors and/or waves) will be filtered out because of its stabilizing designs. The GPS sampling rate does not need to be as high as one for a waverider buoy does. However, it needs additional equipment to record the auxiliary information such as tilt and water line in order to precisely refer the measurements to the actual sea surface. The spar buoy that Born et al. (1994) used in the Harvest T/P calibration site is capable of measuring tilt, temperature, depth and salinity. Also, the antenna height on a spar buoy is generally higher than the one on a waverider buoy; therefore, the former could suffer more multipath effects.

The need for stabilizing devices and additional equipment limits the size of a spar buoy. Alternatively, the waverider buoy is light-weight, small, reusable and easy-to-maneuver. Its rapid and easy deployment is favorable for limited budget operations. Nevertheless, there are several technical issues associated with the use of DGPS buoys of both designs for altimeter calibration: they include (1) the difficulty in accurate kinematic solution with a baseline longer than 30 km, (2) hardware robustness, and (3) other error sources that will be discussed in the following paragraphs.

By having two receivers observing GPS carrier phase (and/or code) observations simultaneously, the relative position from the rover (i.e., GPS buoy) to the reference station can be accurately determined by eliminating the clock errors and other common errors from the double-differenced equations. However, as the baseline goes up, the assumption of tropospheric delays at both the rover and the reference station being the same becomes invalid. For example, Born et al. (1994) suggested the 10-km proximity in the GPS buoy application with carrier phase observations. This limits the GPS buoys to be used only in the coastal regions or near the islands. Han (2000) proposed that the absolute GPS positioning to used in the ocean without the need of reference stations. However, its precision is limited by error sources, including SA (Selective Availability), the interpolated clock errors, troposphere model, and GPS orbit errors.

Hardware robustness includes the capability of the on-board radio modem, robustness of data transmission, power supply, as well as the hardware durability of other sensors that collect auxiliary information such as tilt, temperature, atmospheric pressure and salinity. If the real-time positioning is not required, the data can be post-processed and this could reduce the need of real-time transmission. A waverider buoy was used in this study and was not equipped with any other radio transmission equipments.

Other error sources include the antenna model, multipath, buoy movements (drift, orientation and tilt), shape of dome, water line reading and other errors that are difficult to quantify. The height that a GPS buoy corresponds to is that of the the phase centers and it needs to refer to the water surface. Unfortunately, phase centers for L1 and L2 do not coincide, but vary depending on the elevation of incoming signals. Mader (1999) have calibrated different antennas from the major manufactures and precisely determined the phase center offsets to the antenna reference point (ARP). It is of importance because the height might be different in the magnitude of 10-cm if the wrong antenna model is used. The multipath effects are much smaller if the buoy is mounted close to the sea surface (Rocken et al., 1990). Generally, the multipath effect is greater on a waverider buoy than a spar buoy has because of being close to the sea surface.

When a DGPS buoy is deployed on the altimeter sub-satellite point, it produces several hours of continuous time series of the ssh measurements in the geocentric height system, which can be directly compared with altimeter ssh measurements. Although the vertical positioning precision at each epoch is about 2 cm, the dense (normally 1 Hz) GPS buoy ssh time series provides enough redundancy to improve the precision of the predicted ssh when interpolated at tca. Although its accuracy is still limited by the length of the baseline as well as other technical issues mentioned above, it still demonstrates its potential in altimeter absolute calibration.

### 3.2.2 Tide Gauges

Mitchum (1996) has demonstrated that TOPEX instrument drift can be monitored with an accuracy of less than 1 mm/year using the World Ocean Circulation Experiment (WOCE) tide gauges, most of which are located in the equatorial Pacific. Tide gauges provide continuous, long-term ssh observations that can be utilized in altimeter drift estimation. Whenever the altimetric satellite flies over, a closure equation (3.2) or (3.3) can be established. In addition, the tide gauge data are generally available over the altimeter mission lifetime increasing the redundancy of the closure equations. This results in reducing the drift estimation errors. The primary limitations include that tide gauge calibration of altimeter does not have absolute bias information unless the true datum is known. In addition, the estimated drift from

tide gauges represents the total drift, including drifts from instrument and individual media and geophysical corrections. There are technical issues that have to be considered. It includes (1) height conversion, (2) datum transformation, as well as (3) geoid gradient.

A tide gauge measures the water level changes with respect to a local vertical benchmark. This relation from the gauge to the benchmark is often maintained by spirit leveling and the sea level changes measured by the tide gauge consequently refers to the same vertical datum to which the benchmark refers. Traditionally the horizontal and vertical datums are treated separately and the local mean sea level is normally selected as the zero surface of the vertical reference frame. However, because of conventions, not all tide gauges (or the benchmark that the tide gauge refers to) express the ssh measurements (or their elevations) in the same vertical reference frame. For example, the tide gauge measures ssh in dynamic height.

Generally, the orthometric height is used in representing the vertical elevation of points in surveying. It is the height of a point above the geoid, or mean sea level, along the curved plumb line, whereas the dynamic height of a point is the geopotential number divided by the normal gravity at a parallel (Heiskanen and Moritz, 1987). The dynamic height is defined in Figure (3.2) and equation (3.4):

$$H_{dym} = \frac{C}{g_0}$$
$$C = W_0 - W_P, \tag{3.4}$$

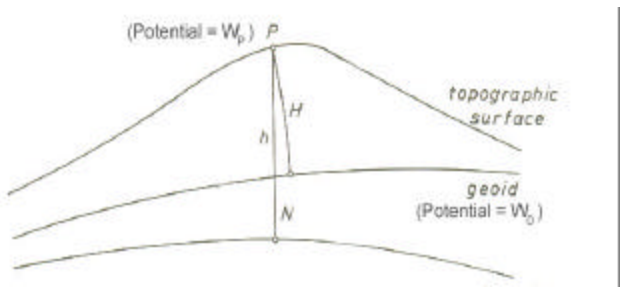


Figure 3.2: The geoid height and potential, (Moritz, 1989).

where $\boldsymbol{C}$ is the geopotential number and $g_0$ is normal gravity at an arbitrary parallel, usually 45° (Heiskanen and Moritz, 1987). $\boldsymbol{W_0}$ is the potential on the geoid and $\boldsymbol{W_P}$ is the potential at the point $\boldsymbol{P}$ on the topographic surface. The geopotential number is the potential difference between geoid to the point $\boldsymbol{P}$.

The difference between the orthometric height and the ellipsoidal height of a point $P$ is called the geoid height. Figure 3.2 and Equation (3.5) demonstrate this relationship:

$$N = h - H \tag{3.5}$$

As illustrated, $\boldsymbol{h}$ is the ellipsoidal height measured along the normal, $\boldsymbol{H}$ is the orthometric height measured along the curved plumb line, and $\boldsymbol{N}$ is the geoid height. Although the plumb line in Figure 3.2 is treated as a straight line, equation (3.5) sufficiently holds to at least the 1st order.

The equipotential surfaces are not parallel to one another, so two points with the same ellipsoidal height might have different dynamic height. In practice, equation (3.6) is used to convert the dynamic height to the orthometric height. That is

$$H = \frac{C}{g + 0.0424H} = \frac{H_{dym} \cdot g_0}{g + 0.0424H} \tag{3.6}$$

where $\boldsymbol{g}$ is is the gravity measured at a ground point and $\boldsymbol{H}$ is the supposed Helmert orthometric height (Heiskanen and Moritz, 1987). It needs to be solved iteratively with the dynamic height $\boldsymbol{H_{dym}}$ being the first approximation of the Helmert orthometric height $\boldsymbol{H}$. With the combination of (3.5) and (3.6), the dynamic heights can be compared with the ellipsoidal ones as long as the geoid height $\boldsymbol{N}$ is known. Geoidal height can be obtained from a number of geoid models or it can be directly calculated by equation (3.5), disregarding the impact of deflections of vertical, with $\boldsymbol{h}$ measured by the GPS buoy near the tide gauge and $\boldsymbol{H}$ obtained from the tide gauge. As a result, the water levels measured by a tide gauge in the dynamic system can now be converted to the geocentric (ellipsoidal) height system. It provides a common ground for the ssh measurements obtained from both the tide gauge and the altimeter so that the closure equation (3.2) or (3.3) can be established.

The other disadvantage of using tide gauges in altimeter calibration is that the gauges might not be on, or within 1-2 km of the altimeter sub-satellite points. Although data from some of the gauges can be tracked back to several decades or longer, their original purpose was not for altimeter calibration and they are not likely to be near the altimeter sub-satellite points either. Also, as mentioned before, the water vapor measurements from the on-board

radiometer are often corrupted by land contamination in the coastal regions, and altimeter ssh measurements can be problematic near the coastal regions. As a result, the tide gauge ssh measurements are required to be extrapolated to where the good altimeter ssh measurements are. This extrapolation is accomplished as the geoid gradient and will be discuss in the next section. Unless the gauge is specifically installed at a calibration site (e.g., Harvest), the geoid gradient could be needed.

One advantage of using tide gauge data as the in situ measurements is that the capability of sea surface height monitoring in a continuous sense. It provides a continuous and long-term time series to be compared with the measurements from the altimeter. This is favorable for the determination of bias drift because with longer time series it is more likely that a precise drift estimation will be obtained.

### 3.3 Geoid Gradient

Geoid gradient is a measure of the change of the sea surface height because of measurements collected at different locations. The in situ ssh measurement is expected to be exactly at the altimetric sub-satellite point when the satellite overflies. If we were to compare the altimeter-measured ssh with GPS data or tide gauge data that were taken elsewhere, we need to account for the geoid gradient. Applying this correction, the altimeter-measured ssh will be "translocated" to where the in situ measurements were taken (or vice versa). In other words, the geoid gradient should be applied to either $h_a$ or $h_i$ in the closure equation (3.2) and (3.3) before the least squares adjustment to determine the altimeter bias and drift. Its magnitude depends upon the displacement between the points and may change in different area. In general, the further the extrapolation, the larger the error. It could dominate other errors if the distance is extremely large. Two possible approaches to account for the geoid gradient will be discussed below. However, other approaches are also possible.

#### 3.3.1 Geoid Gradient Modeled with Bins

The first approach is to model the sea surface with a series of planes, which are next to each other along the altimetric ground track on the sea surface. This method can use the so-called altimeter stackfile (c.f., Guman, 1997; Kruizinga, 1997). For example, T/P repeat ground tracks deviate from the nominal track approximately by ±1 km in the equatorial areas. The distance between two sub-satellite points on the same ground track is approximately 6 km.

Therefore, the small planes that are used to approximate the sea surface are about 6 by 2 km. They are called a *bin* and the geoid gradients within each bin are formulated as in equation (3.7):

$$h_a = \overline{h_a} + x \cdot dx + y \cdot dy + e, \qquad e \sim (0, \Sigma) \tag{3.7}$$

where $\boldsymbol{h_a}$ is altimeter ssh measurement within the bin, $h_a$ is mean ssh of the bin, $\boldsymbol{x}$ and $\boldsymbol{y}$ are along-track and cross-track distances respectively, $d\boldsymbol{x}$ and $d\boldsymbol{y}$ are along-track and cross-track gradients, and $e$ is the random error associated with measurements. Due to the repeat orbit design, $\boldsymbol{h_a}$ in the bin will be accumulated over time but the locations may differ. The unknown parameters $h_a$ , $d\boldsymbol{x}$ and $d\boldsymbol{y}$ can be solved with least squares. $h_a$ becomes the representation of ssh at the bin center. $d\boldsymbol{x}$ and $d\boldsymbol{y}$ are valid only within the bin.

### 3.3.2 Geoid Gradient Modeled with Geostatistical Approaches

The second method to for obtaining the geoid gradient is the geostatistical approach (e.g., least squares collocation or kriging) that provides spatial prediction at the new location. An empirical covariance function is established with the values of all known points in the experimental area (ssh, in this case). The values at the new points are predicted with the empirical covariance function. There are several krigings, for example, simple kriging and ordinary kriging, mentioned in Cressie (1993) that are able to predict the values at the new points and provide the optimal prediction at each new point. It was originally used to predict coal mineral based on limited ground observations and was used in spatial interpolation recently (Cressie, 1993). Hardy (1984) proved that the least squares collocation is a special case of kriging. The values predicted with these geostatistical approaches are consistent with the neighboring points in the experimental area.

The altimeter ssh measurements can then be used to establish an empirical covariance function, based upon which the ssh values at the "new points" are predicted. In other words, if the in situ data sets are not located at altimeter ground tracks, the predicted ssh values at locations where the in situ data sets are taken can be obtained with the geostatistical approaches. Although the along- and cross-track gradients mentioned in Section 3.3.1 may not be explicitly determined with geostatistical approaches, altimeter-measured ssh in the left-hand side of the closure equation (3.2) or (3.3) can be rephrased with a "predicted" ssh for further calculation.

Suppose we have

$$y(s_i) = x(s_i) + e_i, \qquad e_i \sim (0, s_0^2) \qquad Cov\{x(s_i), e_i\} = 0 \tag{3.8}$$

where $\boldsymbol{s_i}$ is a non-random location index. $\boldsymbol{x(s_i)}$ is a noiseless random process to be determined, representing the true value (e.g. true sea surface) at each point $\boldsymbol{s_i}$. $\boldsymbol{y(s_i)}$, another random process, is the observation (e.g. ssh) at point $\boldsymbol{s_i}$. $\boldsymbol{e_i}$ is the random error associated with the observation $\boldsymbol{y(s_i)}$ and it is assumed to be uncorrelated with random process $\boldsymbol{x(s_i)}$. $s_0^2$ is the variance of observations $\boldsymbol{y(s_i)}$. $\boldsymbol{Cov\{\cdot,\cdot\}}$ is covariance between two random arguments. The value $\boldsymbol{x(s_{new})}$ at new point $\boldsymbol{s_{new}}$ can be predicted with the empirical covariance function determined from the observation vector $\boldsymbol{[y(s_1), y(s_2),\ldots, y(s_p)]^T}$.

Supposing there are $p$ points observed, (3.8) can be expressed as a matrix form as (3.9) with $\boldsymbol{y}$, $\boldsymbol{x}$ and $\boldsymbol{e}$ being p-by-1 vectors. $\boldsymbol{I_p}$ is a p-by-p identity matrix. The non-random location index $\boldsymbol{s_i}$ is omitted in the expression for the sake of simplicity.

$$y = x + e, \qquad e \sim (0, \Sigma = s_0^2 \cdot I_p) \qquad Cov\{x, e\} = 0 \tag{3.9}$$

The value $b_x$ denotes the expectation of vector $\boldsymbol{x}$. Since $\boldsymbol{x}$ is a random process but $b_x$ is not, by equating them, there is one more random term needed in the right-hand side in order to carry the randomness. That is

$$b_x = x + e_0, \qquad e_0 \sim (0, \Sigma_x) \tag{3.10}$$

$b_x$ is the covariance of the random vector process $\boldsymbol{x}$ and represents the deviation of $\boldsymbol{x}$ from $b_x$. Consequently (3.9) can be augmented with (3.10) and form a random effect model, which can be solved by least squares.

The covariance function, as mentioned before, is unavailable but it could be estimated empirically by means of (3.11) if random processes $\boldsymbol{x}$ and $\boldsymbol{y}$ are stationary and isotropic. Assuming $\boldsymbol{s}$ and $\boldsymbol{s'}$ are arbitrarily selected locations in the experimental area and $\boldsymbol{s} \neq \boldsymbol{s'}$, a stationary process means that the parallel shift of the arguments $\boldsymbol{(s, s')}$ does not affect moments (e.g., expectation and variance) of the process. For example if we assume $\boldsymbol{x}$ is a stationary

process, the expectation of ***x(s)*** would be the same as the expectation of ***x(s')***. Also, if the orientation of the arguments ***(s, s')*** does not affect moments of the process, it is called isotropic. In other words, the orientation between point pairs does not change the moments of the process.

The covariance estimator between random processes ***y(s)*** and ***y(s')*** separated within a distance $\|s' - s\|$ can be obtained as (3.11) assuming ***y*** is a stationary and isotropic process. Please also note that any predominant trend involved in the random process ***y(s)*** needs to be removed. In the following equation,

$$C(\|s'-s\|) = \frac{1}{k}\sum_{i=1}^{k}[y(s) - b_x]\cdot[y(s') - b_x] \tag{3.11}$$

***k*** denotes the number of pairs with a given lag. Lags do not necessarily have to be equally spaced, buy they have to be appropriately separated so that the number of pairs in each lag could contribute to the estimator. Journel and Huijbregts (1978) suggested at least 30 pairs in each lag. With the information of $C(\|s'-s\|)$ with respect to $\|s'-s\|$, the empirical covariance function can be modeled. According to its characteristics, there are some covariance function models that can be chosen from. For example, the covariance should reach its maximum (i.e., called variance) when the lag distance is zero. Closer neighboring points contribute to a point more than points far from it. In other words, as the distance increases, the covariance value drops rapidly. These characteristics limit the number of candidates. Cressie (1993) provided a list of possible candidate functions. Once a covariance function model is selected, its parameters can be determined with least squares based on the covariance estimators obtained from (3.11). Figure 4.5 and Figure 4.6 illustrate an implementation of using the Gaussian Covariance Function that is used to model geoid gradient in Lake Michigan.

Once the covariance function is determined, $x(s_{new})$ can be predicted with kriging approaches. Simple kriging and ordinary kriging will be discussed in the following. They are different mathematical models but provide prediction at the new point in the optimal sense. However, either one of them should be selected as the best representation (prediction) at the new point. Hypothesis tests between their numerical outputs are required and will be discussed later.

Let $k$, which is a covariance matrix from the new point to all other points, be defined as in (3.12).

$$k = k(s_{new}) = Cov\{x(s_{new}), \begin{bmatrix} y(s_1) \\ y(s_2) \\ \vdots \\ y(s_p) \end{bmatrix}\} \tag{3.12}$$

where ***Cov{ · ,· }*** is covariance between two arguments, which is obtained from the selected covariance function model determined earlier. Also let

$$\begin{aligned} K &= S + Sx \\ \Sigma &= s_0^{\ 2} \cdot I_p, \end{aligned} \tag{3.13}$$

where $S$, the covariance matrix of observations and $S_x$, the covariance of all points, are obtained from the selected covariance function model.

With simple kriging, the new point prediction and associated mean square prediction error (MSPE) can be calculated with (3.14) and (3.15).

$$\tilde{x} = \tilde{x}(s_{new}) = k^T \cdot K^{-1} \cdot (y - t \cdot b_x) + b_x \tag{3.14}$$

$$MSPE\{\tilde{x}\} = \Sigma_0 - k^T \cdot K^{-1} \cdot k \tag{3.15}$$

where $t = [1 \quad 1 \quad \cdots \quad \cdots \quad 1]^T$. It can be seen that (3.14) and (3.15) are equivalent to the least squares collocation with $b_x$ being equal to the mean of the observations. This equivalency also can be found in Hardy (1984).

With ordinary kriging, a primal linear system (3.16) is established with $t = [1 \quad 1 \quad \cdots \quad \cdots \quad 1]^T$, $\boldsymbol{K}$ and $t$ are obtained from the selected covariance function model; see (3.12) and (3.13).

$$\begin{bmatrix} K & -t \\ t & 0 \end{bmatrix} \cdot \begin{bmatrix} c \\ n \end{bmatrix} = \begin{bmatrix} k \\ 1 \end{bmatrix} \tag{3.16}$$

$$\tilde{\tilde{x}} = \tilde{\tilde{x}}(s_{new}) = c^T \cdot y \tag{3.17}$$

$$MSPE\{\tilde{\tilde{x}}\} = \Sigma_x - c^T \cdot k \cdot n \tag{3.18}$$

$$\hat{b}_x = (t^T \cdot K^{-1} \cdot t)^{-1} \cdot t^T \cdot K^{-1} \cdot y \tag{3.19}$$

Solve for $\begin{bmatrix} c & n \end{bmatrix}^T$ in (3.16) then the new point prediction and its MSPE could be obtained by (3.17) and (3.18). $\hat{b}_x$, the estimate of the expectation of $\boldsymbol{x}$, is also determined with (3.19) as the by-product in the ordinary kriging.

$\tilde{x}$ (from simple kriging) and $\tilde{\tilde{c}}$ (from ordinary kriging) are different predictors determined from different mathematical models. One of them ought to be selected as the best prediction at the new point. The following hypothesis tests must be performed in order to test the statistical consistency between both models:

(i) identity test of $b_x$ and $\hat{b}_x$ with a student t test,

(ii) identity test of $\tilde{x}$ and $\tilde{\tilde{c}}$ with a student t test, and,

(iii) variance test of MSPE{ $\tilde{x}$ } and MSPE{ $\tilde{\tilde{c}}$ } with an f-test.

# CHAPTER 4

## LAKE MICHIGAN CAMPAIGN AND DATA ANALYSIS

### 4.1 Lake Michigan Campaign

A GPS buoy campaign in Holland, Michigan was conducted by the Laboratory for Space Geodesy and Remote Sensing Research, Department of Civil and Environmental Engineering and Geodetic Science at the Ohio State University (CEEGS/OSU) in cooperation with the National Geodetic Survey, National Oceanic and Atmospheric Administration (NGS/NOAA) from March 20 to 24, 1999. It was intended to independently measure water levels of Lake Michigan with the GPS buoy and with the Holland West tide gauge for the absolute calibration of TOPEX Side A (TSA) and Side B (TSB). T/P altimeter water level height measurements from MGDR-B database were used. This campaign also planned to calibrate Geosat Fallow-On (GFO) on March 24, 1999 but the results are not reported in this study. In this campaign, Lake Michigan was chosen instead of the ocean (e.g., Born et al., 1994; Morris and Gill, 1994; Hein et al., 1992) because of relatively calm water surface conditions such as wave and wind. Moreover, even though the sea surface height (ssh) is realized as one of the altimeter measurements, the water levels that T/P has measured in this campaign were indeed the lake surfaces. Hence, the water level height will be used, instead of ssh, to refer to this quantity in this chapter in order to better describe the reality.

On the other hand, the in situ water level height measurements from a waverider GPS buoy and from a nearest tide gauge were also collected in order to form the closure equation for T/P bias and/or drift determinations. The preliminary result was published by Cheng et al. (2000). Figure 4.1 illustrates the campaign location and T/P trajectory over the experimental area.

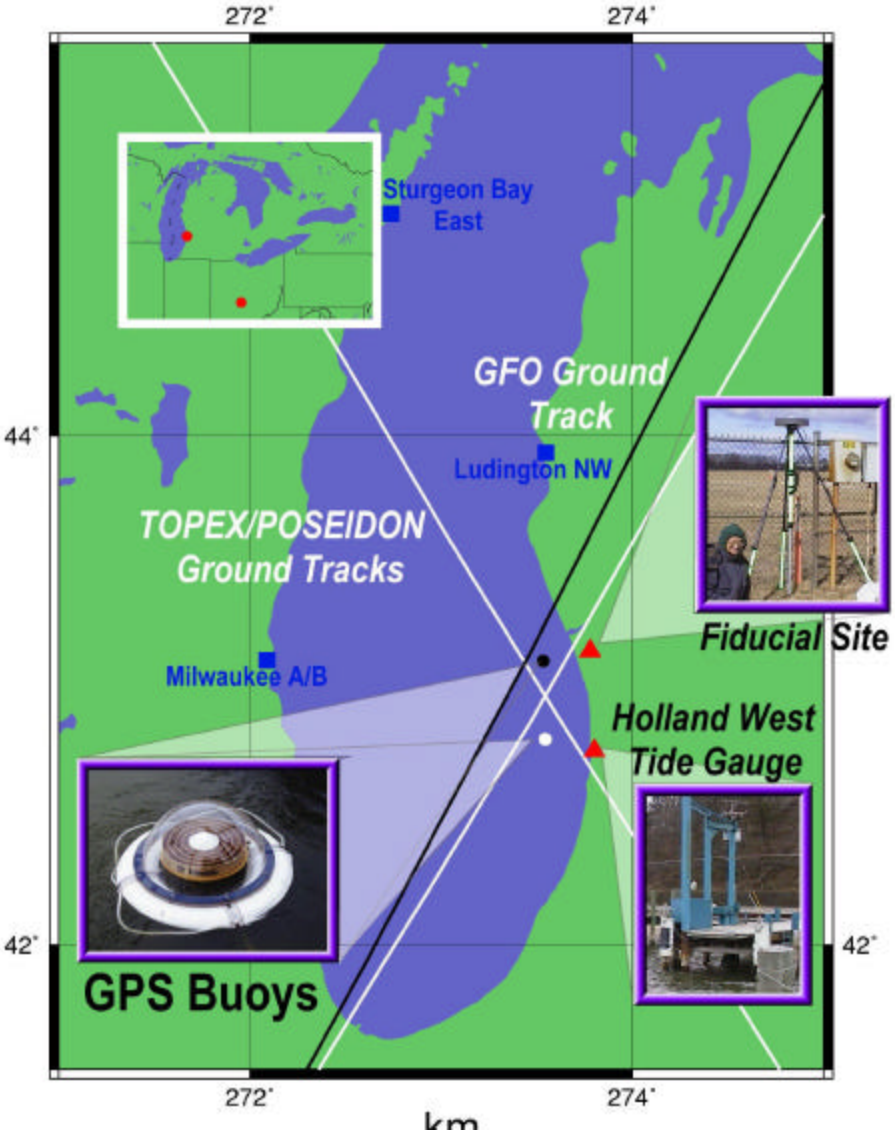


Figure 4.1: Lake Michigan GPS buoy campaign, March 20-24, 1999.

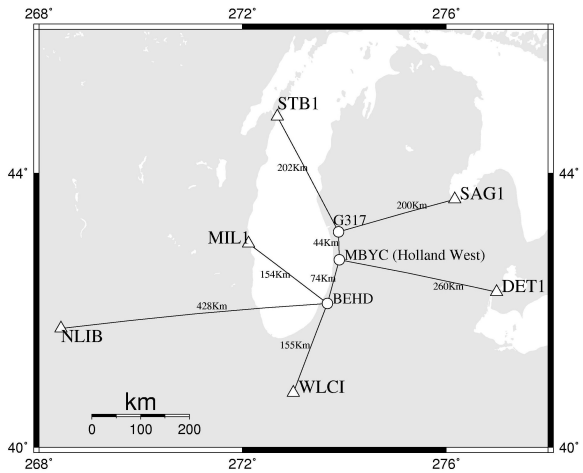


Figure 4.2: GPS network verification for Lake Michigan campaign.

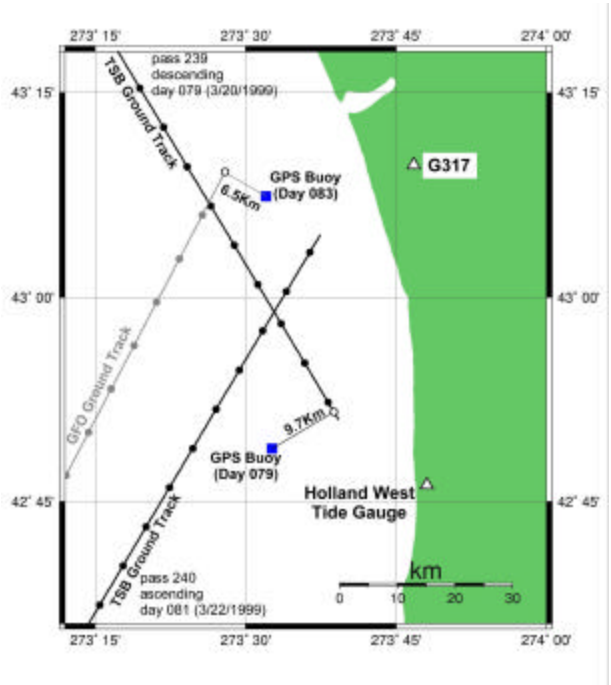


Figure 4.3: GPS buoy deployed locations and TSB ground tracks.

The GPS buoy was planned to be on one of the TSB sub-satellite points in Lake Michigan at cycle 239 on March 20, 1999. Holland West, a NOAA tide gauge benchmark closest to the TSB trajectory was selected as the reference station for the GPS kinematic positioning. It results in an approximate 21-km baseline for the GPS kinematic positioning. GPS buoy data were taken in kinematic (epoch-by-epoch) mode with 1-second rate. A geodetic GPS network verification (will be discussed in Section 4.3) was also performed three months thereafter. The participating stations of the network were carefully selected from IGS and NGS Continuously Operating Reference Station (CORS) in the vicinity.

Figure 4.2 shows the GPS network in the Lake Michigan campaign. Triangles are CORS and circles are new points to be determined. GPS code and carrier phase observations were collected in the static mode for three consecutive days with an 8-hour observing period daily. The absolute position of the Holland West benchmark was then achieved from the GPS network determination.

Figure 4.3 illustrates the actual GPS buoy deployed location and the TSB trajectories. Solid dots represent the 1-Hz TSB sub-satellite points and the empty dots are the points of the closest approach (i.e., the shortest distance from GPS buoy deployed location to T/P trajectory). The GPS buoy location was anticipated to be on the T/P ground track but due to inaccurate orbit prediction and communication errors, it was off by 9.7 km. This displacement caused a significant geoid gradient effect from the actual buoy deployed location to the sub-satellite point. Therefore, a geoid gradient correction was applied to the altimeter water level height measurements to translocate them to the GPS buoy location. As it will be shown later, this error produces the predominant error for the final altimeter bias estimation. The details will be discussed in Section 4.2.

In addition to the GPS buoy, the tide gauges also provide the height measurements for radar altimeter absolute calibration. However, due to the relatively large footprint of the on-board radiometer, radar altimeters do not provide accurate water level height measurements near the coast. The use of tide gauges in altimeter absolute calibration requires an accurate knowledge of the local geoid, or a rigorous numerical inter/extrapolation such as one of the geostatistical approaches mentioned in Section 3.3.2. Moreover, the tide gauge normally refers to a local vertical datum, which is not consistent with the one that the radar altimeter refers to. Therefore, height conversion and a vertical datum transformation are required in order to make use of tide gauge data in radar altimeter absolute calibration. The Holland West tide gauge, which is the tide gauge in the experimental area nearest (still about 21 km off) to the good T/P water level height measurement, was selected in this campaign for TSA and TSB calibration. A spatial extrapolation was performed to account for the geoid gradient. The GPS buoy was deployed near the tide gauge (within about 30 meters) in order to provide the geocentric height information needed for vertical datum transformation.

In the following sections, the water level heights from T/P, the GPS buoy and the Holland West tide gauge will be discussed in detail. Geoid, or mean lake level, gradient corrections were applied to T/P water level height measurements, which will be discussed in

Section 4.2. The altimeter bias and drift estimations and corresponding error budgets will be discussed in Section 4.4 and 4.5. The fieldwork logs can be found in the Appendix A.

## 4.2 Altimeter-Derived Water Levels

Due to the land contamination with the large (~40 km) footprint of the on-board radiometer, the T/P water level height measurements near the coast are not reliable. There is a flag in the MGDR (Merged Geophysical Data Record-B) that indicates the reliability of each T/P measurements. For that reason, the last TSB sub-satellite point in the descending pass 239 (the last solid dot on the descending pass in Figure 4.3) was selected as the calibration location for GPS buoy deployment. Unfortunately, the GPS buoy was not accurately deployed at the designated calibration location and was off by about 9.7 km. Consequently, the calibration location was forced to move to 42° 51' 35.7084" N and 273° 38' 47.4144" E (the lower empty dot in Figure 4.3), which were the coordinates of the sub-satellite point on T/P trajectory closest to the buoy. The time of closest approach (tca), the time when satellite passed over this selected sub-satellite point, was 82952 seconds of the day on March 20, 1999.

TSB altimeter water level height measurements are retrieved from the MGDR-B database, which is a T/P data product set that includes measurements from on-board altimeters and the TOPEX Microwave Radiometer (TMR). Its global data coverage is between latitudes ± 66 degrees and its ground track pattern repeats within ± 1km every 9.99156 days. The sea surface height (or water level height in the inland lakes) above the T/P reference ellipsoid is one of the main parameters from this dataset. Benada and Digby (1997) discussed MGDR-B in full details.

In a generic case of radar altimeter absolute calibration, a calibration location could be one of the sub-satellite points where the water level height from altimeter and in situ both are available at the same time (such as measurements from GPS buoys or tide gauges). If the buoy is not precisely deployed on the selected calibration location, the sub-satellite point closest to the buoy will be selected as the calibration location and a geoid gradient correction is required. The time that the satellite flies over the calibration location is often called "time of closest approach (tca)" and it is also the time that the calibration is performed. Since the sampling epochs in both T/P and GPS are not synchronized, 10-Hz raw T/P water level heights are often used. They are necessary to be smoothed with a low-pass filter in order to reduce high-frequency errors and the random noise. The altimeter water level height at tca is consequently predicted based on the raw measurements after the low-pass filtering. Corrections mentioned in Section 2.3 need to be applied to the raw altimeter measurements to

adjust to the realistic water level situation. However, tidal variations were retained in altimeter ssh because the same variations exist in the GPS buoy and tide gauge measurements as well.

As mentioned before, the actual GPS buoy location was 9.7 km off the T/P overflight location. This displacement results in the need for a geoid, or lake surface gradient correction to translocate the altimeter-derived water level height measurements to the location of the GPS buoy measurement. This gradient correction is the water level height change due to different locations and can be solved by using an accurate geoid model or a rigorous numerical spatial inter/extrapolation approach.

Figure 4.4 illustrates the geoidal height indicated by other geoid models at the points along pass 239 as well as the water level heights measured by TSB. It indicates a significant shape difference in the TSB water level height measurements. Although this difference may include the propagating error by removing the means of each data set and fixing them at the 44° latitude, it inevitably shows that the water surface measured by TSB was not consistent with the one indicated by those geoid models. Thus, numerical spatial inter/extrapolations are adopted, such as geostatistical approaches mentioned in Section 3.3.2. In order to account for the geoid gradient, altimeter water level height measurements on the descending pass 239 (on March 20, day of the year: 079) and the ascending pass 240 (on March 22, day of the year: 081) were collected together to provide adequate geometry for the spatial inter/extrapolation. They were the two closest passes to the tca epoch and should properly reflect the lake hydrological phenomena. An empirical covariance function was determined based on all TSB water level height measurements on these two passes. Consequently, the TSB water level height at GPS buoy deployed location was predicted according to the empirical covariance function (See Section 3.3.2 for detail formulas). Apparently, if the buoy had been accurately deployed, the geoid gradient would have been avoided. This gradient certainly introduced one more error source to the altimeter bias estimations.

The Gaussian covariance function (illustrated in Figure 4.5) was selected as the empirical model for least squares curve-fitting. TSB water level heights on both passes 239 and 240 were taken as the observations, $y$, which implicitly includes the random process, $x$, and the random error, $e$, in Equation (3.8). Covariance estimators were collected with (3.11) and with a 20-km lag length. The empirical covariance function was then determined by the least squares with the number of pairs in each lag as the weight. According to Journel and Huijbregts (1978), 30 pairs are at least needed to contribute sufficiently to the covariance estimators; the weight in the categories that has less than 30 data pairs were purposely set to 0.1. Figure 4.6 illustrates the result of curve-fitting and the weighting strategy. Other functions such as the Gauss-Markov covariance functions with different orders were also tested. However, by comparing with the variance component of each covariance function after least squares curve-fitting, the other covariance functions do not prevail. The estimated parameters after the least squares are also listed in Figure 4.5.

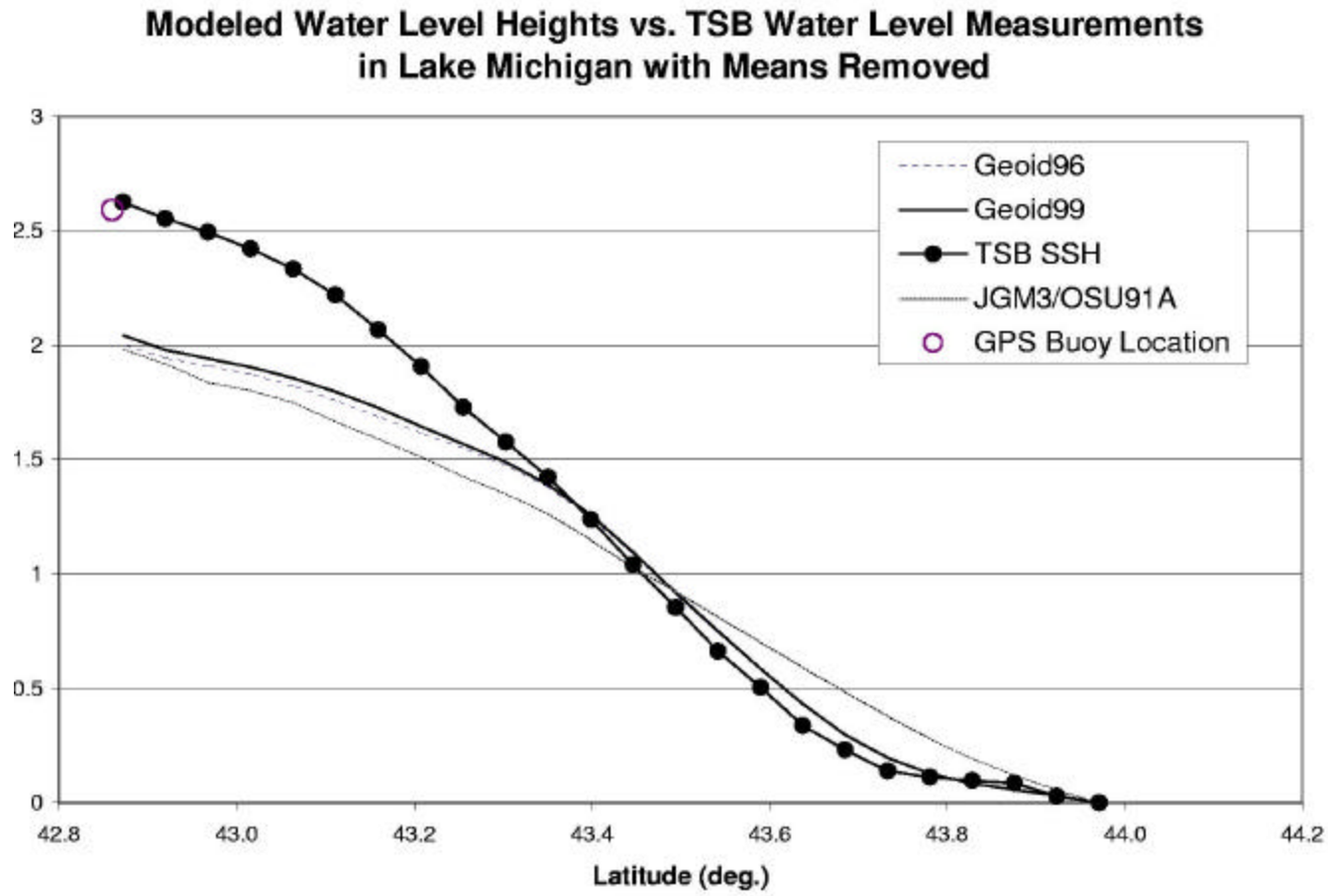


Figure 4.4: A relative comparison (mean-removed) of the water level heights indicated by geoid models and measured by TSB at the points on the pass 239.

Gaussian Covariance Function :

$$C(s) = C_0 \cdot \exp(-b^2 \cdot s^2)$$

where $C(s)$ is covariance between two arbitrary point pair,

$s$ is the lag distance between pair,

$C_0$ is variance, and,

$b$ is correlation distance.

$C_0 = 281.403223\ 80198359\ \ \mathrm{m}^2$ and

$b = 0.00699402\ 82$ (unitless)

were estimated after least squares adjustment.

The dispersion matrix of the paremeters is : $\begin{bmatrix} 33.42851e+001 & 9.503872e-004 \\ 9.503872e-004 & 6.918564e-008 \end{bmatrix}$

Figure 4.5: Gaussian covariance function and its numerical result based on TSB water level heights on the pass 239 and the pass 240

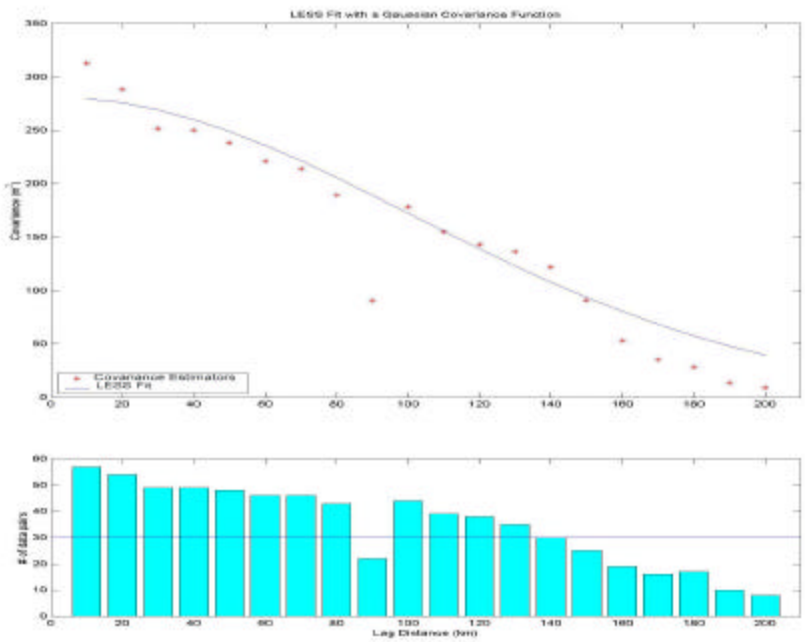


.

Figure 4.6: Least squares curve-fitting with a Gaussian covariance function (above) with TSB water level heights on the pass 239 and the pass 240. The number of data pairs in each lag is used as the weight (below). Note the weight will be set to 0.1 if the number of data pairs in a lag is less than 30.

The TSB water level height prediction at the GPS buoy deployed location (42° 48' 54.5477" N, 273° 32' 38.8405" E.) was then predicted based on the empirical Gaussian covariance function that has been determined above. Two types of predictor and the associated hypothesis tests were performed. Figure 4.7 illustrates the numerical result of the hypothesis tests. $\beta_x$ is an arbitrary trend of all observations. Since all observations were greater than 139.50 m, this value was then removed from all observations for the simplicity of the numerical calculation in simple kriging. $\hat{\beta}_x$ is the mean of all observations that is estimated with ordinary kriging. $\check{x}$ and $\bar{\check{x}}$ are the water level height predictions at the GPS buoy deployed location and are predicted with the simple kriging and the ordinary kriging respectively. MSPE stands for the Mean Square Prediction Error and is MSPE { • } the mean square prediction error of the random process •. After analyzing hypothesis tests with 95 % confidence level, the results of the simple kriging and the ordinary kriging are not significantly different. Therefore, the simple kriging predictor, $\check{x}$ = 142.351 ± 0.157 m, was selected to represent the TSB water level height prediction at the GPS buoy deployed location. Figure 4.8 presents the MSPE plot verse east longitude. It indicates the MSPE of simple kriging over the experimental area.

Simple Kriging :

$\beta_x \quad = 139.500$ m (given).

$\tilde{x} \quad = 142.351044 \pm 0.157015$ m

$MSPE\{\tilde{x}\} = 0.02465366\ \mathrm{m}^2$

Ordinary Kriging :

$\hat{\beta}_x \quad = 141.764 \pm 10.207677$ m (estimated).

$\tilde{\tilde{x}} \quad = 142.344633 \pm 0.159652$ m

$MSPE\{\tilde{\tilde{x}}\} = 0.02548875\ \mathrm{m}^2$

Hypothesis Tests :

(i) identity test between $\beta_x$ and $\hat{\beta}_x$ , (t - test).

H0 : $\beta_x == \hat{\beta}_x$.

$T_1 = 0.2219,$

$t_{97.5\%}(49) = 2.0096,\ t_{2.5\%}(49) = -2.0096.$

Accept H0.

(ii) identity test between $\tilde{x}$ and $\tilde{\tilde{x}}$, (t - test).

H0 : $\tilde{x} == \tilde{\tilde{x}},$

$T_2 = -0.0286,$

$t_{97.5\%}(97) = 1.9847,\ t_{2.5\%}(97) = -1.9847$

Accept H0.

(iii) improvment test between $MSPE\{\tilde{x}\}$ and $MSPE\{\tilde{\tilde{x}}\}$, (f - test).

H0 : $MSPE\{\tilde{x}\} == MSPE\{\tilde{\tilde{x}}\},$

$T_3 = 1.0380,$

$f_{95\%}(48,49) = 1.6102,$

Accept H0.

Figure 4.7: Hypothesis tests of TSB water level height prediction at GPS buoy deployed location by the simple kriging and the ordinary kriging.

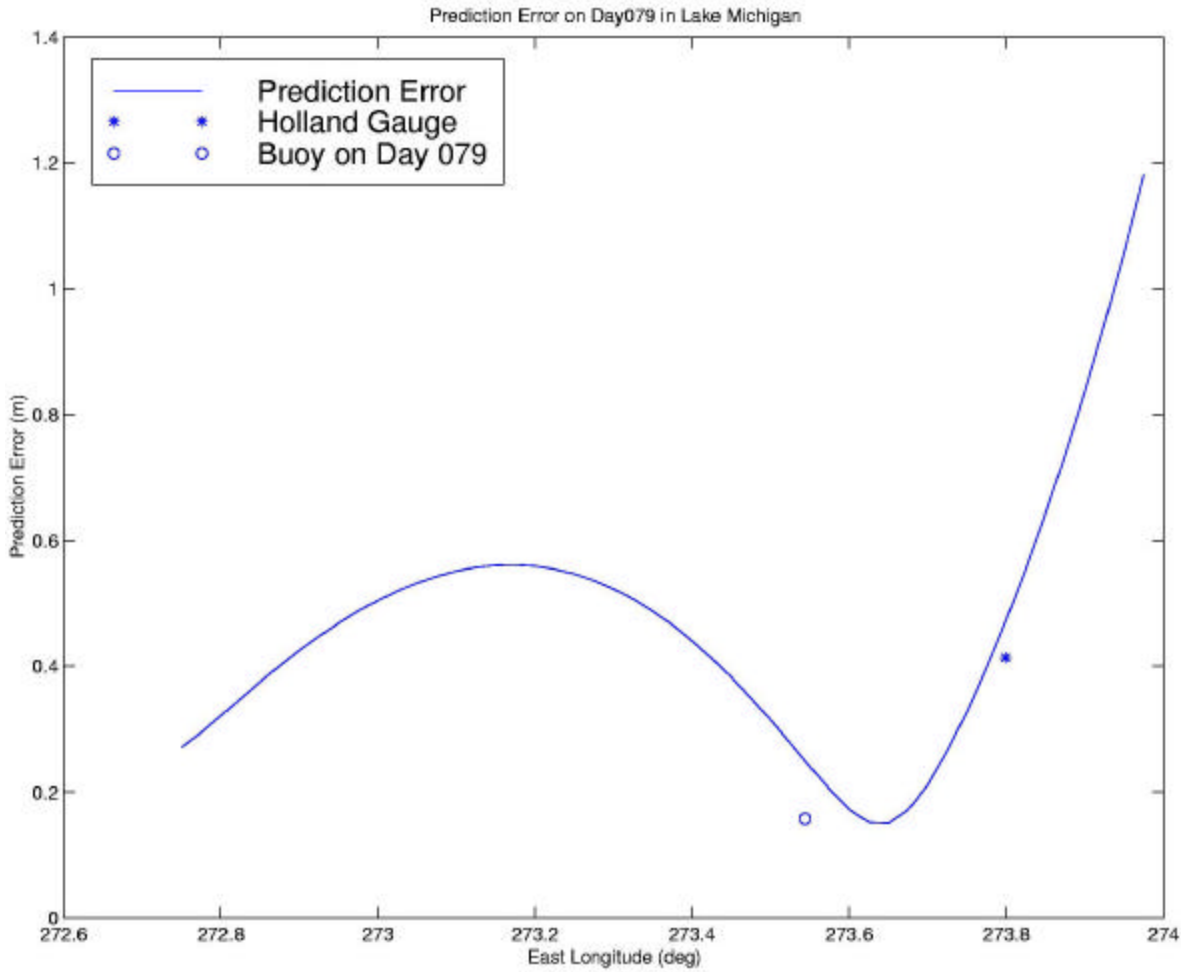


Figure 4.8: The prediction error of the simple kriging over Lake Michigan.

### 4.3 GPS-Derived Water Levels

A GPS geodetic network, as illustrated in Figure 4.2, was established with the IGS/NGS CORS in the vicinity. Snow (2001) has verified the published (booked values) coordinates of all participating CORS and determined the coordinates of the new points (G317, BEHD and Holland West) with the weighted partial MInimum NOrm LEast Squares Solution (MINOLESS). The adjusted coordinates and associated standard errors of the Holland West monument are listed in Table 4.1. The reference ellipsoid is T/P reference ellipsoid with semi-major and flattering being 6378136.3 m and 1/298.257 respectively (Born et al., 1994).

The GPS buoy data (phase and code observations) was collected at 1-second rate in the kinematic (epoch-by-epoch) mode with respect to the Holland West monument whose coordinates were computed from the geodetic network above. The GPS buoy (as illustrated in Figure 4.9) was built by attaching a geodetic-quality choke ring antenna with a floater buoy with a plastic transparent dome on top. The offset between the antenna reference point (ARP) and the buoy water line was carefully measured indoors and in a nearby pier with all equipments on board. As a result, the ellipsoidal height of the ARP could actually refer to the water level where the buoy was deployed.

The software used in this study is KARS (Kinematic And Rapid Static) developed by Mader (1986). It was specifically developed for high-precision GPS kinematic positioning. In this study, the ionosphere-free phase solution, which is a linear combination of L1 and L2 phase observations that eliminates the ionospheric delays, was achieved. The antenna models developed by Mader (1999) at NGS/NOAA were used to account for the phase centers variation (can be around 10 cm vertically if using the wrong antenna type). Moreover, the IGS precise orbits (2-week ephemeride) were also used to ensure the positioning accuracy. The kinematic solutions were then converted into ITRF96, which T/P refers to. Then in order to reduce the effect of waves, the data was smoothed with the low-pass filter such as the polynomial-fit in different order with different window sizes (1-, 10-, 30- and 60-minute centered at tca). Under 95% confidence level, the estimated GPS water level at tca was selected as 142.297 ± 0.002 m with one-hour window size. Table 4.2 illustrates the result after data-smoothing. Figure 4.10 demonstrates the estimated GPS water level at tca with the 60-min data.

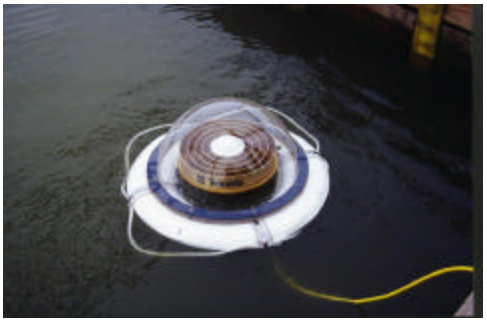

Figure 4.9: The waverider buoy used in the Lake Michigan campaign.

| Coordinates | X (m) | Y (m) | Z (m) | Latitude (deg.) | Longitude (deg.) | h (m) |
|---|---|---|---|---|---|---|
| Holland West | 310880.092 | -4679085.777 | 4308925.669 | 42.4614130 | -86.1155806 | 143.245 |

| Variances | X (mm) | Y (mm) | Z (mm) | Latitude (arcsec.) | Longitude (arcsec.) | h (mm) |
|---|---|---|---|---|---|---|
| Holland West | 3.4 | 19.3 | 17.3 | 0.00013 | 0.00015 | 25.6 |

Table 4.1: Coordinates and associated standard errors of the Holland West monument in the T/P reference ellipsoid (Snow, 2001).

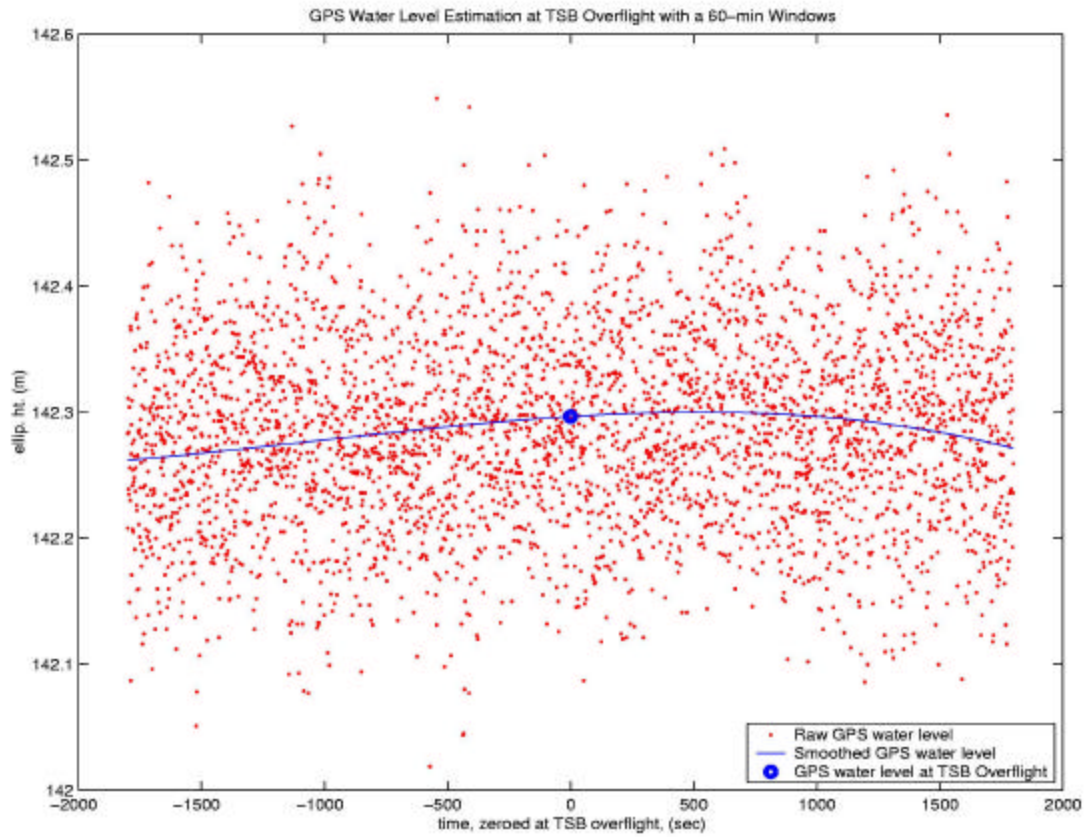


Figure 4.10: GPS water level estimation at TSB overflying epoch (tca) with a 60-minute window.

### 4.4 Error Budget of Altimeter Bias Estimated with GPS Buoy Data

Christensen et al. (1994) and Kruizinga (1997) studied the possible error sources in altimeter bias estimation and categorized them into fixed errors and variable errors in a temporal sense. The fixed error pertains to the repeatable component and the variable error pertains to the time-dependent nature of the bias estimation from pass to pass. Hence, an increasing number of independent estimations will reduce the impact of the variable errors but the fixed errors can only be reduced by accurate calibrations (Christensen et al., 1994) or perhaps by averaging calibration (closure) samples from multiple calibration sites in different locations of the world ocean.

With the numerical results from the previous two sections as well as the error analyses of Christensen et al. (1994) and Kruizinga (1997), the error budget of TSB altimeter bias estimation in this study is presented in Table 4.3. A similar table is given by Kruizinga (1997).

Table 4.3 also includes the GPS buoy error budget. Reference station errors were estimated by means of the weighted MINOLESS of the GPS geodetic network as mentioned in Section 4.3. Variable error in relative positioning was merely from the random error indicated by the polynomial fit of GPS kinematic data, whereas the fixed error is speculated as 20 mm containing fixed "mis-modeled" error from curve fitting. Errors from antenna tilt and multipath would not affect a waverider buoy as much as they do a spar buoy. These errors depend on the antenna height from the water surface and elevations of the incoming GPS signals and need to be accounted for if a spar buoy is used. Errors of the antenna height measurements could be affected by the errors of the height measurements in the laboratory and the errors of the waterline. The latter one depends on the water density and salinity at deployment. Both fixed and variable errors were speculated with data of the precision of the metal ruler that was used. The decorrelation sampling error, the deviation of the mean wave to the true mean water level, depends on the magnitude of waves. As mentioned before, the period of waves is around 2-20 seconds and much shorter in the shallow water. A 1-Hz GPS sampling rate should be in the safe side especially the water level height of GPS were taken in a lake.

As a result, assuming all error sources are independent, the altimeter bias estimation is 54 mm with a total error (RSS, root sum squares of all errors) of 169 mm. Geoid gradient error (157 mm) that is caused by the 9.7-km offset between T/P sub-satellite point at tca to the GPS buoy deployed location, should be the most dominant error source that could have been avoided. That is, if the GPS buoy has been deployed accurately on the T/P sub-satellite point, the bias estimation error could have been improved to 62 mm. Although this 62-mm accuracy does not reach the accuracy needed for altimeter bias determination (less than 1-cm accuracy in bias estimation), it is anticipated that the accuracy of bias estimation could be reduced with

more GPS buoy measurements in the future. In the next section, the possible reduction of variable errors will be demonstrated using the water level time series from the Holland West tide gauge to calibrate the TSA altimeter measured lake level over a 7-year data span.

| Error Sources | Fixed (mm) | Variable (mm) | RSS (mm) |
|---|---|---|---|
| Altimeter | | | |
| Radial orbit | 20 | 10 | |
| Noise | - | 20 | |
| Instrument(s) | 11 | 20 | |
| Dry tropospheric delay | 2 | 7 | |
| Wet tropospheric delay | 5 | 18 | |
| Ionospheric delay | 10 | 5 | |
| EM bias | 10 | 14 | |
| Total altimeter errors | 27 | 39 | 47 |
| Geoid gradient | 157 | - | 157 |
| Total altimeter error with geoid gradient | 159 | 39 | 164 |
| GPS buoy | | | |
| Reference stations | 20 | 26 | |
| Relative positioning | 20 | 2 | |
| Antenna Tilt | - | - | |
| Multipath | - | - | |
| Antenna Height Measurement | 10 | 2 | |
| Decorrelation sampling | - | - | |
| Total GPS buoy errors | 30 | 26 | 40 |
| Total bias estimation error with geoid gradient | | | 169 |
| Total bias estimation error without geoid gradient | | | 62 |

Table 4.3: Error budget of TSB altimeter bias estimation with the GPS buoy water level height measurements.

## 4.5 Error Budget of Altimeter Bias Estimated with Tide Gauge Data

As mentioned in Section 3.2.2, the use of tide gauge in the satellite radar altimeter absolute calibration needs to consider three main technical issues: (1) height conversion, (2) datum transformation, and (3) geoid gradient. The following passage will implement these three steps with data from the Holland West tide gauge, the one that is closest (~21 km) to the good altimeter water level height measurements in Lake Michigan.

(1) Height Conversion

The water level information from 1992 to 1999 provided by the Holland West tide gauge, located near Holland, Michigan, were provided in the International Great Lakes Datum 1985 (IGLD 85), a dynamic height system. Data from 1992 to 1998 are hourly-averaged and data from 1999 are only daily-averaged. The data history covers the TSA mission and the beginning of the TSB mission continuously, but with some small gaps. Therefore, these data sets were used in this study for altimeter bias and drift determinations of TSA and TSB.

Since the dynamic height does not measure geometric distance, equation (3.6) was applied to convert the water level height measurements from the dynamic height to the Helmert orthometric height. Figure 4.11 presents the difference between these two vertical datums at Holland West with data from 1992 to 1999. The difference through time is varying and its magnitude is about 0.4 mm.

(2) Datum Transformation

The water level height measurements of T/P refer to the T/P reference ellipsoid with the semi-major axis and flattering being 6378136.3 m and 1/298.257 respectively (Born et al., 1994). The in situ data set, water level height from Holland West tide gauge, inevitably needs to convert to the same vertical system in order to form the closure equations. In order to convert water level height measurements of the Holland West tide gauge from Helmert orthometric heights to the ellipsoidal heights, the geoid height, $N$ in (3.5), at the tide gauge needs to be accurately known. It can be derived from the accurate local geoid models or can be directly measured by a GPS buoy deployed by the tide gauge. However, the geoid models that used in Figure 4.4 indicate that the water levels they refer to are not consistent to the one that T/P measured. Therefore, the GPS buoy measurements by the tide gauge are adopted as the alternative.

The GPS buoy was deployed near (~30 m) the tide gauge to directly measure the water level at the gauge in the "ellipsoidal" heights. The data were taken in a 3-hour session for two days. On the other hand, the tide gauge readings in the dynamic height system were converted into the orthometric in the previous step. At the result, the local geoid height can be solved

with (3.5) and it was consequently applied to the tide gauge data to convert them to the geocentric height, to which T/P water level height measurements refer. This conversion provides a common ground to establish a closure equation "at the tide gauge" when both T/P and tide gauge data were available.

(3) Geoid Gradient

Geoid, or mean lake surface, gradient correction is needed whenever the water level height measurements of the in situ data set are not exactly on the T/P trajectory. It needs to be applied to either altimeter-measured or to the in situ data set when establishing a closure equation. Due to the dynamic variance of the altimeter measurements near the coasts, the T/P water level height measurements close to the tide gauge are unreliable. The closure equations need to be established where good T/P water level measurements are. Hence, the water level measurements from a number of nominal T/P sub-satellite points were selected as illustrated in Figure 4.12. The geoid gradient correction in each T/P visit was determined with the geostatistical approach individually and was applied to the altimeter water level measurement. Considering that annual signals and semi-annual signals implicitly contribute to both date sets, the closure equation (3.3) was used in each altimeter overflies in order to account for these signals. The absolute comparison of the water level measurements from T/P with geoid gradient correction applied and from the Holland West tide gauge is presented in Figure 4.13. Table 4.4 presents the numerical result of T/P altimeter bias and drift determinations with least squares. Apparently, there seems to be a 10-cm discrepancy involved in Figure 4.13, which may be caused in part by the inaccurate datum transformation using GPS buoy measurements. However, the altimeter bias drifts are still solvable in this case and they are presented in Figure 4.14 with means of the water level height measurements from both data sets removed.

Apparently, TSB bias drift estimations are not consistent with TSA because of the number of the redundant closure equations. The redundancies in TSA and TSB drift determinations are 112 and 13 respectively. The number of the available closure equations in TSB drift determination is inadequate so that TSB drift estimation was not reported in Table 4.4. By comparing the bias estimation errors of TSA and TSB, the power of redundancy in reducing the estimation errors is evident. Even though the estimation errors in TSB are not satisfying, they will hopefully improve by establishing more closure equations in the future.

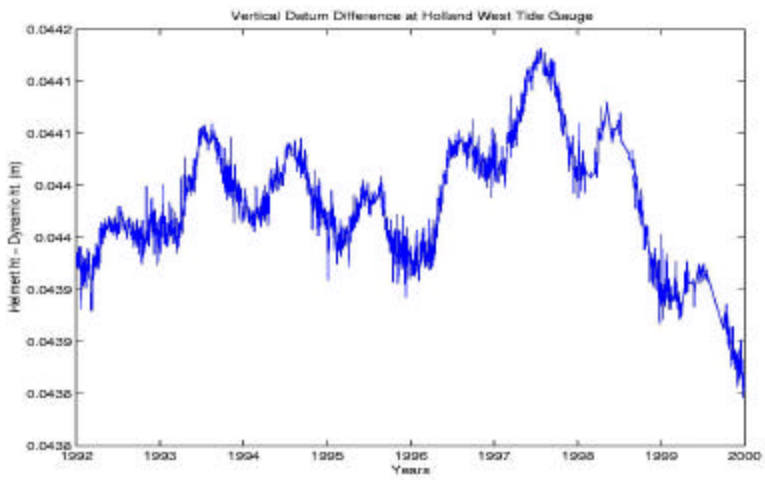


Figure 4.11: Height difference (Helmert orthometric height – Dynamic height) at the Holland West tide gauge with data from 1992 – 1999.

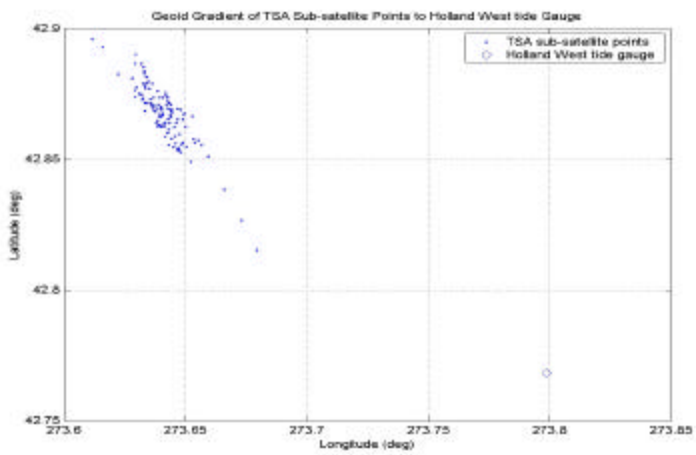


Figure 4.12: The locations of T/P nominal sub-satellite points and the location of the Holland West tide gauge.

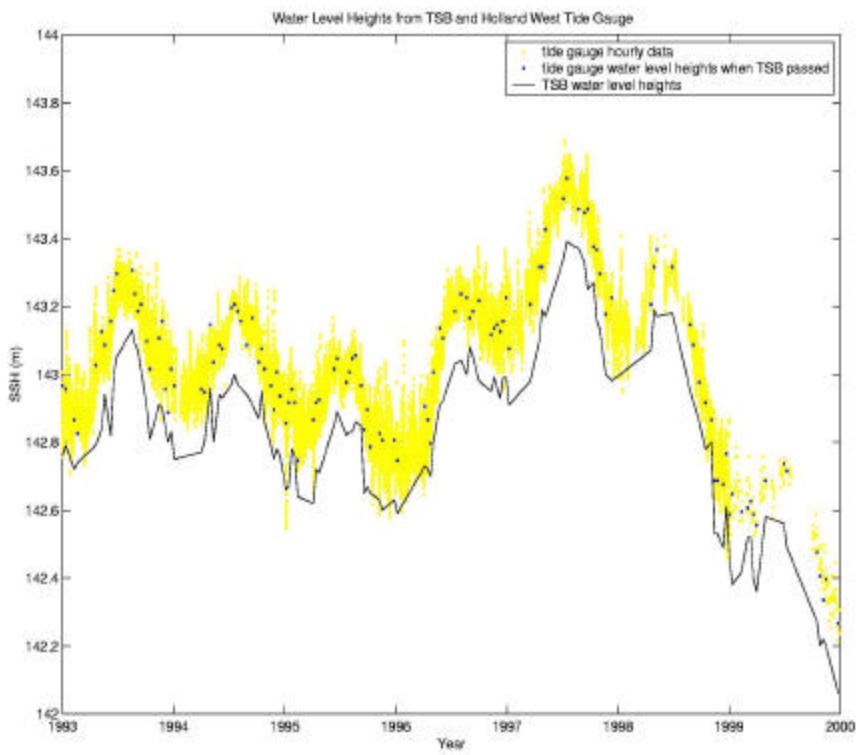


Figure 4.13: An absolute water level height comparison between T/P and the Holland West tide gauge on T/P reference ellipsoid. The geoid gradient in each individual closure equation has applied to the T/P water level height measurement.

| | TSA | TSB |
|---|---|---|
| Bias Estimate | -22.5 ± 8.3 mm | 65.9 ± 72.6 mm |
| Drift Estimate | 4.4 ± 2.5 mm/year | N/A |

Table 4.4: T/P altimeter bias and drift estimations with the in situ water level data from the Holland West tide gauge from 1993 – 1999. TSB drift estimation is not reported because the calibration samples in TSB were inadequate.

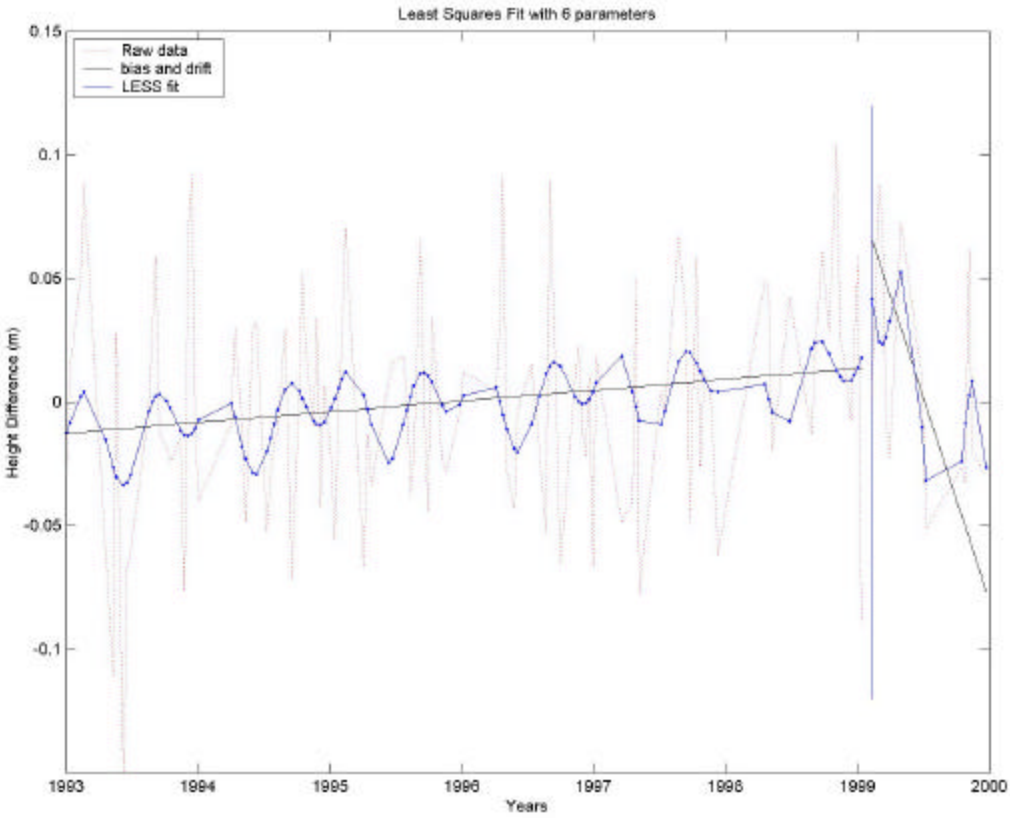


Figure 4.14: T/P bias drift estimations with water level height (mean-removed) measurements from the Holland West tide gauge. The closure equation with annual and semi-annual parameter was used in least squares curve-fitting.

| Error Sources | Fixed (mm) | Variable (mm) | RSS (mm) |
|---|---|---|---|
| Altimeter | | | |
| Radial orbit | 20 | 10 | |
| Noise | - | 20 | |
| Instrument | 11 | 20 | |
| Dry tropospheric correction | 2 | 7 | |
| Wet tropospheric correction | 5 | 18 | |
| Ionospheric correction | 10 | 5 | |
| EM bias | 10 | 14 | |
| Total altimeter errors | 27 | 39 | 47 |
| Geoid gradient | 431 | 3 | 431 |
| Total altimeter error with geoid gradient | 432 | 39 | 434 |
| Holland West tide gauge | | | |
| Gauge reading | - | 10 | |
| Height conversion | 30 | 5 | |
| Gauge noise | - | 20 | |
| GPS benchmark survey | 20 | 26 | |
| Leveling | 10 | 10 | |
| Total tide gauge error | 37 | 36 | 52 |
| Total bias estimation error with one closure equation | | | 437 |
| Total bias estimation error (TSA) with all (112) closure equations | | | 41 |

Table 4.5: Error budget of TSA bias estimation with water level height measurements from the Holland West tide gauge.

Table 4.5 is the error budget of TSA bias estimation with 112 closure equations. The random (variable) error in gauge reading depends on the type of the gauge and also on the observers' attention. The Holland West is a traditional gauge that requires observers to occasionally read it manually. The 10-mm random error is a safe speculation. This error could be improved using more modern tide gauges. Geoid height at the tide gauge was determined by a direct comparison of the ellipsoidal height measured by the GPS buoy and the orthometric height converted by Equation (3.6). The fixed and variable errors in height conversion contain the errors from both the practical formula as well as the GPS buoy measurements. Again, the values were speculated based upon both results. The gauge noise is a random quantity that depends on the instrument. Since the factory-calibrated value was unavailable, a centimeter level accuracy should be a reasonable guess. The Holland West benchmark serves as the reference station in GPS buoy kinematic positioning. Hence the errors in the benchmark should be the same as the reference station errors in Table 4.3. Leveling provides the connection from the tide gauge to the Holland West benchmark. Errors associated with it are as a function of distance from the gauge to the benchmark (about 500 m in this case). Hence, the random (variable) error of leveling should be as small as 10 mm in order to be compliance with the surveying standard. Fixed error in level is the systematic error of the spike rod. The 10-mm fixed error is a conservative speculation.

## 4.6 Summary

The technique to determine TSA and TSB altimeter bias and drift were implemented in this chapter using the in situ data from a GPS waverider buoy and the Holland West tide gauge in Lake Michigan GPS Buoy Campaign in 1999. GPS buoy data were used to form a closure equation sample on March 20 and to help datum transformation for the Holland West tide gauge. The TSA and TSB bias and drift estimations were listed in Table 4.4. Due to the 10-cm discrepancy in the Holland West tide gauge ssh, both bias estimations are inaccurate. Also, the TSB drift estimation was not reported because of the inadequate number of closure equation samples collected in TSB mission. Hence, the only one reasonable result is the TSA altimeter drift estimation: $4.4 \pm 2.5$ mm/year. Haines et al. (1998) reported the TSA altimeter drift estimation of $1.0 \pm 1.9$ mm/year with 5-year continuous data from Harvest calibration site.

It is anticipated that the estimation errors would be improved with more calibration samples collected and incorporated. As mentioned before, the required accuracy in the bias and drift estimations are less than 1 cm and 1 mm/year respectively. Figure 4.15 speculates the necessary calibration sites and calibration samples to achieve the required 1-cm accuracy in the altimeter bias estimation assuming other calibration sites are independently located in a

different geographical area and also assuming that the in situ data accuracy is similar to the ones in the Lake Michigan Campaign.

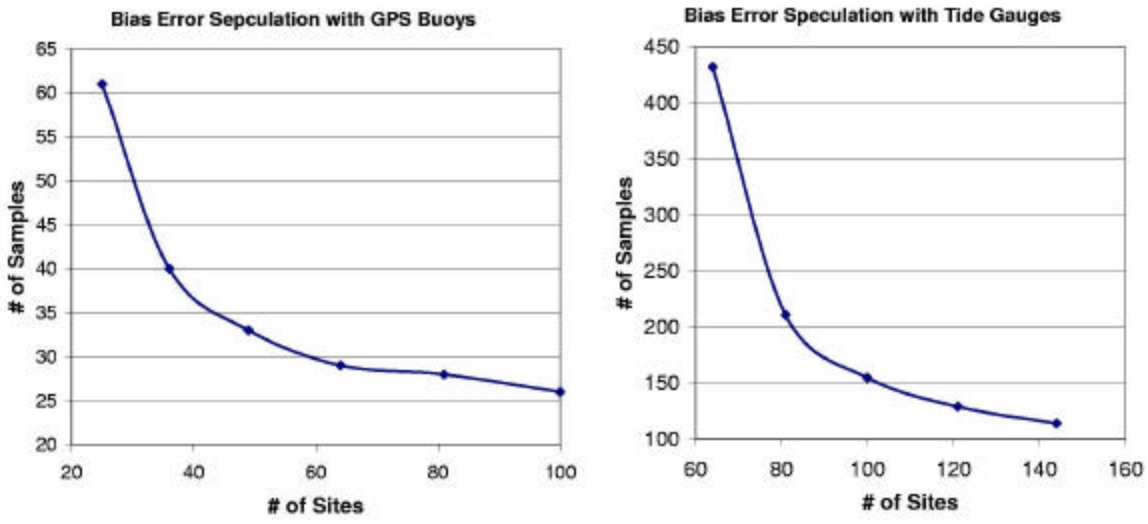


Figure 4.15: Altimeter bias error speculations with GPS buoy data (left) and tide gauge data (right).

# CHAPTER 5

## CONCLUSION

The altimeter bias and its drift are the closure between the altimeter-measured ssh and the ground truth, both of which contain errors. The required accuracies of altimeter bias and drift are 1cm and less than 1 mm per year that are inherently required for the use of a radar altimeter to measure the global mean sea level. The determinations of bias and drift are the determinations of the secular and the time-varying closure between altimeter-measured ssh and the ground truth. GPS buoys and tide gauges provide the ssh in different fashions but are both capable of being the in situ data sets for satellite radar altimeter absolute calibrations.

Lake Michigan GPS buoy campaign demonstrates a generic example of the satellite radar altimeter absolute calibration. The lake was chosen in the campaign because of the relatively calm water conditions such as waves and wind. It shows that a GPS waverider buoy facilitates the absolute radar altimeter calibration with the advantage of being small-sized, reusable, easy-to-maneuver and accurate. Geoid (or mean lake surface) gradient correction in this campaign is the crucial point that dominants other error sources (~ ± 157 mm over a 9.7-km arc distance). It could have been eliminated if the GPS buoy was accurately deployed on the T/P trajectory. Building an autonomous, near-permanent GPS buoy for the long-term water level monitoring is possible if the corresponding hardware issues, such as the capability of radio modems, robustness of data transmission, power supply and hardware durability are resolved. GPS geodetic network verification and analysis are required especially when the reference stations are located at unstable areas where the vertical motions cannot be ignored. Proximity of the GPS buoy to the reference station is always essential. The combination of TSB altimeter bias, error sources as described in Table 4.3, and the random noise in this campaign is 54 ± 169 mm. Assuming the GPS buoy were deployed correctly on the T/P trajectory the combination of those quantities could have been improved to 54 ± 62 mm.

The Holland West tide gauge, on the other hand, provides continuous long-term water level time series for altimeter bias and drift determinations by forming 111 and 13 closure equations for the computation in TSA and TSB respectively. The TSA bias and drift estimations are –22.5 ± 8.3 mm and 4.4 ± 2.5 mm/year respectively. The TSA bias estimation here, however, do not reflect the bias because of the 10-cm discrepancy between the water level height measurements from T/P and from the Holland West tide gauge. This

discrepancy is seemingly caused by the unknown reasons in height conversion and datum transformation. The TSB bias estimation (66 ± 73 mm) is not accurate because of the inadequate number of closure equation samples collected. It would be improved with more valid closure equation samples collected in the future. It can be concluded that the ssh measurements from tide gauges can be useful in the drift determinations even if there is obviously a discrepancy between the altimeter-measured ssh and in the tide gauge ssh data set.

The geoid, or mean sea surface, gradient correction in the use of tide gauge to altimeter calibration also dominates other error sources. This is inevitably difficult to prevent because of the unreliability of the altimeter ssh measurements near the coastal areas. Unless few designated tide gauges (e.g., Harvest) are specifically installed on the altimeter trajectory for absolute calibration, the geoid gradient correction is unavoidable for most of the tide gauges. However, with the advantages of being reusable, easy-to-maneuver and accurate, the GPS buoys can be deployed at the points between the tide gauges and the desirable altimeter trajectories. The GPS buoy ssh measurements can be, in turn, utilized to measure ssh change among the location of the altimeter footprint, the location of the tide gauge, and locations in between. They will give us better understanding in making geoid, or mean sea surface, gradient corrections. This could reduce the impact of the geoid, or mean sea surface, gradient for most of tide gauges to a more satisfying extent. However, an accurate local geoid model is expected and further studies on this issue are required.

Although each individual ssh measurements from either GPS buoys or from the Holland West tide gauge in this study do not sufficiently reach mm-level accuracy, it can be anticipated that the accuracy of the altimeter bias and drift estimations could still be improved with more closure equation samples established in the future as more data is being collected. GPS buoys and tide gauges serve as the in situ data sets in providing the independent ssh measurements to the radar altimeter absolute calibration. Other technologies are still possible in providing similar data; for example, bottom pressure gauges. The problems left are accuracy, convenience and costs. It can be seen that the accuracy of the altimeter bias and drift estimations would also be improved with closure equation samples established at other calibration stations worldwide, or even established by other technologies that provide independent and precise ssh measurements.

REFERENCES


Benada. R, and S. Digby, *TOPEX/POSEIDON Altimeter Merged Geophysical Data Record Generation B,* JPL PO.DAAC 068.D002.

Born, G.H, M.E. Parke, P. Axelrad, K.L. Gold, J. Johnson, K. W. Key, and D.G. Kubitschek (1994), Calibration of the TOPEX Altimeter using GPS Buoy, *J. Geophys. Res*., 99, (C12), pp. 24517-24526.

Calman, Y. (1987), Introduction to Sea-surface Topography from Satellite Altimetry, *Johns Hopkins APL Technical Digest,* 8, No. 2, pp. 206-211.

Cheng, K., C.K. Shum, C. Han, M. Parke, Y. Yi, J. Benjamin, G. Mader and D. Martin (2000), GPS-Buoy Water Level Instrument: Applications for Radar Altimeter Calibration, poster, IAG International Symposium on Gravity, Geodesy and Geodynamics 2000, Banff, Alberta, Canada, August.

Cressie, N.A. (1993), *Statistics for Spatial Data*, Revised Edition, A Wiley-Interscience Publication, New York.

Christensen, E.J., B.J. Haines, S.J. Keihm, C.S. Morris, R.A. Norman, G.H. Purcell, B.G. Williams, B.D. Wilson, G.H. Born, M.E. Parke, S.K. Gill, C.K. Shum, B.D. Tapley, R. Kolenkiewicz, and R.S. Nerem (1994), Calibration of TOPEX/POSEIDON at Platform Harvest, *J. Geophys*, pp. 24465-24485.

Dorandeu, J. and P.Y. Le Tron (1999), Effects of Global Mean Atmospheric Pressure Variations on Mean Sea Level Changes from TOPEX/POSEIDON, *Amer. Met. Soc.,* Notes and Correspondence, pp. 1279 – 1283.

Douglas, B. (1997), Global Sea Rise: A Redetermination, *Surveys in Geophysics,* 18, pp. 279-292.

Douglas, B. (1991), Global Sea Level Rise, *J. Geophys. Res.,*96 (C4), pp. 6981-6992.

Fu., L.L., E.J. Christensin, C.A. Yamarone, M. Lefebvre, Y. Menard, M. Dorrer and P. Escudier (1994), TOPEX/POSEIDON Mission Overview, *J. Geophys. Res.,*99 (C12), pp. 24369-24381.

Gaspar, P., F. Ogor, P.Y. Le Traon and O.Z. Zanife (1994), Estimating the Sea State Bias for the TOPEX and POSEIDON Altimeters from Crossover Differences, *J. Geophys. Res.*, 99, (C12), pp. 24981-24994.

Guman, M.D. (1997), Determination of Global Mean Sea Level Variations Using Multi-Satellite Altimetry, *Ph.D. dissertation*, the University of Texas at Austin.

Haines, B., G. Born, E. Christensen, S. Gill and D. Kubitschek (1998), The Harvest Experiment: TOPEX/POSEIDON Absolute Calibration Results from Five Years of

Continuous Data, *AVISO Altimetry Newsletter 6*, http://sirius-ci.cst.cnes.fr:8090/HTML/information/frames/kiosque/news_uk.html, Archiving, Validation and Interpretation of Satellites Oceanographic data.

Han, S.C. (2000), *Static and Kinematic Absolute GPS Positioning and Satellite Clock Error Estimation*, master thesis, the Ohio State University.

Hardy, R.L. (1984), Kriging, Collocation, and Biharmonic Models for Application in the Earth Science, Technical Papers, American Congress on Surveying and Mapping, 44th Annual Meeting, Washington, D. C., pp. 363 - 372.

Hayne, G.S. and D.W. Hancock (2000), *Topex Side B Sigma0 Calibration Table Adjustment*, NASA, Goddard Space Flight Center, Wallops Flight Facility.

Hayne, G.S (1999), *Topex Altimeter Range Stability Estimate Update*, http://topex.wff.nasa.gov/docs/RangeStabUpdate.html, NASA GSFC Wallop Flight Facility, Observational Science Branch, Wallops Flight Facility, Wallops Island, VA

Hein, G.W., H. Blomenhofer, H. Landau and E. Taveira (1992), Measuring Sea Level Changes Using GPS in Buoys, *Sea Level Changes: Determination and Effects*, Geophysical Monograph 90, IUGG Vol. 11.

Heiskanen, W.A. and H. Moritz (1987), *Physical Geodesy*, reprinted, Institute of Physical Geodesy, Technical University, Graz, Austria.

Morris, C.S. and S.K. Gill, (1994), Evaluation of the TOPEX/POSEIDON Altimeter System Over the Great Lakes, *J. Geophys. Res.*, 99, (C12), pp. 24527-24539.

Leick, A. (1995), *GPS Satellite Surveying*, second ed., John Wiley & Sons, Inc, New York.

Lisitzen, E. (1974), Sea Level Changes, *Elsevier Oceanographic Series*, 8, New York.

Lorell, J., E. Colquitt and R.J. Anderle (1982), Ionospheric Correction for SEASAT Altimeter Height Measurement., *J. Geophys. Res.*, 87, (C5), pp. 3207 – 3212.

Journel, A.G. and C.J. Huijbregts (1978), *Mining Geostatistics*, Academic Press, London. p. 194.

Kaula, W.M. (1969), *The Terrestrial Environment: Solid Earth and Ocean Physics*, NASA Rep. Study at Williamstown, MA, NASA CR-1579.

Kelecy, T.M., G.H. Born, M.E. Parke and C. Rocken (1994), Precise Mean Sea Level Measurements using the Global Positioning System, *J. Geophys. Res.*, 99, (C4), pp. 7951-7959.

Kruizinga, G.L. (1997), Validation and Applications of Satellite Radar Altimetry, *Ph.D. dissertation*, the University of Texas at Austin.

Mader., G.L. (1986), Dynamic Positioning Using Global Positioning System Carrier Phase measurements, *Manuscr. Geod.*, 11, pp. 272-277.

Mader, G. (1999), GPS Antenna Calibration at the National Geodetic Survey, *GPS Solutions*, Vol. 3, No 1.

Menard, Y., E. Jeansou and P. Vincent (1994), Calibration of the TOPEX/POSEIDON Altimeters over Lampedusa, Additional Results over Harvest, *J. Geophys. Res.*, 99, (C12), pp. 24487 – 24504.

Mitchum, G.T. (1996), Monitoring the Stability of Satellite Altimeters with Tide Gauges, *J. Atmospheric and Oceanic Technology*, 15, (3).

Moritz, H. (1989), *Advanced Physical Geodesy*, 2nd ed., Herbert Wichmann Verlag GhbH, Karlsruhe.

Ponte, R.M. (1993), Variability in a Homogeneous Global Ocean Forced by Barometric Pressure, *Dyn. Atmos. Oceans*, 18, pp. 209-234.

Peltier, W.R. (1996), Global Sea Level Rise and Glacial Isostatic Adjustments: An Analysis of Data from the East Coast of North America, *Geophys. Res. Lett.*, 23, pp. 717-720.

Rocken, C, T.M. Kelecy, G.H. Born, L.E. Young, G.H. Purcell Jr., and S.K. Wolf (1990), Measuring Precise Sea Level from a Buoy Using the Global Positioning System, *Geophysical Research Letters*, 17, (12), pp. 2145 – 2148.

Schutz, B.E., G. Kruizinga, D. Kuang, P.A. Abusali, C.K. Shum, R. Gutierrez, S. Nelson and E. Rodriguez (1995), Galveston Bay Experiment for Altimeter Calibration, AGU Fall Meeting, San Francisco.

Seeber, G. (1993), *Satellite Geodesy, Fundamentals, Methods, and Applications*, Walter de Gruyter, New York.

Shum, C.K., M.E. Parke and D. Martin (1999), Absolute Calibration and Verification of Multiple Radar Altimeter, *Proc. Intergovernmental Oceanographic Commission Group of Experts Sixth Session on the Global Sea Level Observing System*, Toulouse, France.

Snow, K. (2001) Alternate Adjustment Techniques for Ellipsoid Height Estimates and Accuracy of GPS-Derived Ellipsoid Heights Verses Baseline Length, *master thesis*, the Ohio State University, Columbus, Ohio, USA.

Tapley, B.D., J.B. Lundberg, and G.H. Born (1982), The SEASAT Altimeter Wet Tropospheric Range Correction, *J. Geophys. Res.*, 87, (C5), pp. 3213 – 3220.

Trupin, A, and J. Wahr (1990), Spectroscopic Analysis of Global tide Gauges Sea Level Data, *Geophys. J. Int.*, 100, pp. 441-453.

TOPEX Team (2000), *Special Report, Side B Testing Status*, http://topex.wff.nasa.gov/sideb_status.html, NASA GSFC Wallop Flight Facility, Observational Science Branch, Wallops Flight Facility, Wallops Island, VA.

Urban, T.J. (2000), The Integration and Applications of Multi-Satellite Radar Altimetry, *Ph.D. dissertation*, The University of Texas at Austin.

Warrick, R.A. and J. Oerlemans (1990), Sea Level Rise, In *Climate Changes: The IPCC Scientific Assessment*, J.T. Houghton, G.J. Jenkins and J.J. Ephraums (eds.). Cambridge University Press, Cambridge.

White, E.J., R. Coleman and J.A. Church (1994), A Southern Hemisphere Verification for the TOPEX/POSEIDON Satellite Altimeter Mission, *J. Geophys. Res.*, pp. 24505-24516.

Zilkoski, D.B, J.D. D' Onofrio, R.J. Fury, C.L. Smith, L.C. Huff and B.J. Gallagher (1996), *The U.S. Coast Guard Buoy Tender Test*, Report on the Joint Coast Survey and National Geodetic Survey Centimeter-Level Positioning of a marine Vessel Project, http://www.ngs.noaa.gov/initiatives/HeightMod/Buttonwood/.

APPENDIX A

LAKE MICHIGAN ALTIMETER CALIBRATION CAMPAIGN FIELD WORK LOGS

**Background**

The general purpose of this campaign is to measure the lake level with a special designed GPS buoy in order to compare the lake surface height from the altimeters and the tide gauge data. Two of the crossover points from Topex/Poseidon and GFO in the Lake Michigan near Holland, MI were chosen. The overflight schedule is:

| | | |
|---|---|---|
| T/P | ascending | 2300 UTC, March 20, 1999. |
| T/P | descending | 1154 UTC, March 22, 1999. |

Crossover point: latitude 42-48-51.12N, longitude 86-27-24.48W.

| | | |
|---|---|---|
| GFO | descending | 1618 UCT, March 24, 1999. |
| GFO | ascending | 0157 UCT, March 25, 1999. |

One NOAA benchmark, 7031D was also chosen as the main reference site for the whole campaign. Also a chosen 7031H was also chosen as the auxiliary reference site but has been discarded due to the bad satellite availability. The reason that these two were chosen is because of the availability of reliable knowledge about the relative elevation to the tide gauge. The coordinates for 7031D are:

X: 310880.617 m
Y: -4679087.195 m
Z: 4308925.762 m
Ellipsoidal height:144.37 m
Normal height: 177.74 m.

One Ashtech Z Surveyor and two Trimble 4700 receivers. One choke ring antenna has been sitting on the buoy. The logging rate is 1 second for GPS receivers with 15-degree cutoff mask. The conversion of UTC to the local time is subtracting 5 hours from UTC.

**Participants**

M. Parke, campaign leader, OSU

C. K. Shum, campaign leader, OSU
D. Martin, Coast Survey Development Lab., National Ocean Service, NOAA.
B. Burns, captain, Great Lakes Environmental Research Lab., NOAA.
H. Tseng, OSU
K. Cheng, OSU
J. Shum, OSU/video specialist, UT

**Field Log**

March 18:

- M. Parke left for Holland

March 19:

- M. Parke setup the buoy and a Choke ring antenna. Other participants arrived at Holland. Check all instruments and charged all batteries.

March 20 (DOY 079)

- This session was design for the overflight at 6 pm of T/P satellite. It was tentatively scheduled from 2pm to 7pm.
- M. Parke and H. Tseng took the ship to T/P crossover point and C. K. Shum, D. Martin and K. Cheng went to the main reference sites.
- The Ashtech Z Surveyor series receiver was set at 7031D by 1 pm. The antenna height (choke ring) is 2 meters vertically. Another auxiliary reference site named TOPEX was chosen near 7031D, instead of 7031H. It was not a real monument and was arbitrarily chosen for practice only. A Trimble 4700 was used and its antenna height (micro-center antenna) is 1.927 meters (slant distance). It was started by 1:30 pm; unfortunately, the data was only for 15 minutes due to the hardware problem. The Ashtech receiver choked by 5 pm with an uncertainty of the connection between the receiver to the laptop. D. Martin switched logged data to a flash memory card to solve the problem.
- GPS buoy started tracking data from 3 pm and ended by 7 pm with approximately 3 MB data.

March 21 (DOY 080)

- Data downloading and exchange.
- Fix the buoy, changed a new doom.
- Practice Trimble 4700.

March 22 (DOY 081)

- Cancelled the original plan to occupy the T/P crossover point at 5:54 am because of weather conditions.
- Set Ashtech at 7031D at 1 pm again (Choke ring, 2 meters vertically) and deployed the buoy in the harbor near the tide gauge.

March 23 (DOY 082)

- Occupied 7031D with Ashtech by 11 am. Choke ring, 2 meters vertically.
- Occupied TOP1TX with Trimble 4700 by 1130 am. Micro-center antenna, 1.526 meters uncorrected slant.
- Deployed buoy at the same place by 1130 am.
- Scouted for a new reference site for GFO crossover point.

March 24 (DOY 083)

- Occupied G317 with Ashtech from 1030 am to 1215 pm. That is NOAA's GPS monument near the airport.
- Occupied PARK with Trimble 4700 from 1040 am to 1230 pm. That is an arbitrarily chosen auxiliary points in a park near the beach. The main reason is to reduce the baseline to GFO cross over point. The approximately distance is off 20 kilometers.
- Deployed GPS buoy at the GFO crossover point. It tangled with anchor by 1030 am. There were still 15 to 20 minutes of good data before that.

APPENDIX B

LIST OF ACRONYMS

| | |
|---|---|
| AGC | Automatic Gain Control |
| ARP | Antenna Reference Point |
| AVISO | Archiving, Validation and Interpretation of Satellites Oceanographic data |
| CEEGS/OSU | Civil and Environmental Engineering and Geodetic Science, the Ohio State University |
| CNES | Centre National d' Etudes Spatiales |
| DGPS | Differential GPS |
| DORIS | Doppler Orbitography by Radiopositioning Integrated on Satellite |
| DOY | Day of the year |
| ENVISAT | ENVIronment SATellite |
| ERS | European Remote Sensing satellite |
| ESA | European Space Agency |
| GEOS-3 | Geodetic and Earth Orbiting Satellite 3 |
| GEOSAT ERM | Geodetic Satellite Exact Repeat Mission |
| GEOSAT GM | Geodetic Satellite Geodetic Mission |
| GFO | GOESAT Follow-On |
| GPS | Global Positioning System |
| IB | Inverted Barometer |
| IGLD | International Great Lake Datum |
| ITRF | International Terrestrial Reference Frame |
| JGM | Joint Gravity Model |
| KARS | Kinematic And Rapid Static |
| MGDR | Merged Geophysical Data Record |
| MINOLESS | MInimum NOrm LEast Squares Solution |
| MSPE | Mean Square Prediction Error |
| NASA | National Aeronautics and Space Administration |
| NAVSTAR GPS | NAVigation System with Time And Ranging Global Positioning System |
| NGS | National Geodetic Survey |
| NOAA | National Oceanic and Atmospheric Administration |
| NPOESS | National Polar-orbiting Operational Environmental Satellite System |

| | |
|---|---|
| RSS | Root Sum Squares |
| SLR | Satellite Laser Ranging |
| SSB | Sea State Bias |
| SSH | Sea Surface Height |
| SST | Sea Surface Topography |
| SWH | Significant Wave Height |
| TCA | Time of Closest Approach |
| TMR | Topex Microwave Radiometer |
| TOPEX | TOPography EXperiment |
| TSA | TOPEX Side A |
| TSB | TOPEX Side B |
| SA | Selective Availability |
| WGS 1984 | World Geodetic System 1984 |
| | WOCE World Ocean Circulation Experiment |